Acta Pharmaceutica Sinica B 2025;15(4):2095−2113

Chinese Pharmaceutical Association
Institute of Materia Medica, Chinese Academy of Medical Sciences

Acta Pharmaceutica Sinica B

www.elsevier.com/locate/apsb
www.sciencedirect.com

ORIGINAL ARTICLE

Spermidine inactivates proteasome activity and enhances ferroptosis in prostate cancer

Dan Feng[a], Jian Zhang[b], Huanmin Niu[b], Xiaoxue Zheng[b], Mengqi Jia[b], Qiqi Lu[b], Jing Wang[b], Wenxue Guo[b], Qi Sun[b], Huiqing Yuan[b,*], Hongxiang Lou[a,c,*]

[a]*Department of Natural Medicinal Chemistry and Pharmacognosy, School of Pharmacy, Qingdao University, Qingdao 266071, China*
[b]*Institute of Medical Sciences of the Second Hospital, Cheeloo College of Medicine, Shandong University, Jinan 250033, China*
[c]*Department of Natural Product Chemistry, Key Laboratory of Chemical Biology of Ministry of Education, School of Pharmaceutical Sciences, Shandong University, Jinan 250012, China*

Received 18 April 2024; received in revised form 26 September 2024; accepted 20 December 2024

KEY WORDS

Spermidine;
Proteasome;
Ferroptosis;
EIF5A;
NRF2;
Prostate cancer;
Polyamines;
HMOX1

Abstract The elevated polyamines, amine-rich molecules with diverse functions in pathophysiology processes, are implicated in contributing to tumorigenesis and progression. Whether and how they affect the efficacy of chemotherapy is incompletely understood. Our screening assays reveal that the supplement with a low dose of spermidine (Spd), one of the polyamines, enhances ferroptosis in prostate cancer cells as evidenced by increased lipid peroxidation and intracellular Fe^{2+} levels *in vitro*. Combination treatment with Spd and a low dose of ferroptosis inducer erastin synergistically augments anti-tumor efficacy with undetectable toxicity in mice. Analysis of RNA-seq data indicates that heme oxygenase 1 (HMOX1), an enzyme that catalyzes the cleavage of heme to release Fe^{2+}, is significantly upregulated in response to Spd and erastin cotreatment. Spd mediated the hypusine modification of the eukaryotic initiation factor 5A (EIF5A) promotes the translation of the nuclear factor erythroid 2-related factor 2 (NRF2), subsequently leading to elevation of HMOX1. Moreover, Spd and erastin significantly inhibit proteasome activity which results in a decrease in proteasomal degradation of NRF2, although many proteasome-related genes are induced either by Spd or Spd plus erastin. Thus, in addition to its pro-oncogenic activity, the supplement of Spd improves antitumor activity in combination with ferroptosis inducers and offers an optional approach to cancer treatment.

*Corresponding authors.
E-mail addresses: louhongxiang@sdu.edu.cn (Hongxiang Lou), lyuanhq@sdu.edu.cn (Huiqing Yuan).

Peer review under the responsibility of Chinese Pharmaceutical Association and Institute of Materia Medica, Chinese Academy of Medical Sciences.

https://doi.org/10.1016/j.apsb.2025.02.023

1. Introduction

Despite the great achievements made in cancer treatment, resistance to therapy, particularly to chemotherapy, remains a major contributor to cancer recurrence that eventually leads to failure in the successful treatment. Chemotherapy is a primary treatment for cancer, particularly for metastatic tumors, resistance to various chemotherapeutic drugs is inevitable and causes poor survival outcomes and complications in patients[1-3]. For example, the first line therapy for castration-resistant prostate cancer (CRPC) is docetaxel-based chemotherapy, almost all patients eventually develop resistance after one year of treatment, despite a good response and survival benefit observed initially. Few therapeutic approaches are available to CRPC patients progressing to docetaxel resistance[4]. Resistance to chemotherapy has been reported for almost all the drugs used clinically. Therefore, a number of studies have focused on the identification of novel therapeutics for reversing drug resistance or the development of optional approaches to enhance chemosensitivity.

Polyamines are amine-rich and positively charged molecules, including putrescine (Put), spermidine (Spd), and spermine (Spm). They are natural mammalian polyamines and exert diverse functions in normal cells due to their specialty in structures that allow them to easily interact with negatively charged molecules, such as proteins and nucleic acids, and affect biological processes[5]. In addition to influencing protein/DNA interactions, polyamine-mediated protein modification is also unique in biological processes. It is demonstrated that Spd contributes to the hypusination of the eukaryotic translation factor 5A (EIF5A), which is essential for the synthesis of many proteins including transcriptional factors, oncogenic proteins, and epigenetic modifiers involved in the regulation of proliferation, senescence, inflammation, and immune system. Therefore, the dysfunctional metabolism of polyamines is closely correlated with the development of diseases. The elevated polyamines and their biosynthetic genes are frequently observed in various cancers and positively contribute to the severity of malignancy[6,7]. Therefore, Blockade of polyamine metabolism results in the suppression of tumor growth and provides an option for cancer therapy[6,8]. Several inhibitors of the polyamine biosynthesis enzymes and polyamine transporters have been identified. Difluoromethylornithine (DFMO), an irreversible inhibitor of the rate-limiting enzyme of the polyamine biosynthesis named ornithine decarboxylase (ODC), is able to deplete Put and Spd accompanied by growth inhibition in cancer[9]. Moreover, the combination of DFMO combined with other agents, for example, with 5-azacytidine (a demethylating agent) also increases M1 macrophages in the tumor microenvironment, and increases antitumor efficacy in an ovarian cancer mouse model[10]. Recent investigations highlight an interesting role of polyamines in cancer immunotherapy. Spd supplementation enhances the antitumor activity of PD-1 blockade immunotherapy in mice. The study defines that Spd directly binds to mitochondrial trifunctional protein (MTP) and activates fatty acid oxidation (FAO) in T cells[11]. This suggests that polyamines, besides their promoting effects on tumor growth, may control the inflammatory response to immunotherapies, and have complicated roles in balancing tumor malignancy and anti-tumor efficiency. Whether the antitumor effect of polyamines is specific in some types of cancers or ubiquitous in most cancers, and whether they affect the efficacy of various chemotherapeutics in cancer treatment remains to be elucidated.

In this study, we found that Put, Spd, and Spm had limited effects on the cytotoxic activity of chemotherapeutic reagents that are often clinically used in various cancer cells. However, Spd significantly sensitized erastin-induced ferroptosis in prostate cancer cells by increasing intracellular ferrous ions. This effect of Spd depended on the inhibition of proteasome activity and facilitating hypusine modification of EIF5A, which results in the accumulation of nuclear factor erythroid 2-related factor 2 (NRF2) and activation of heme oxygenase 1 (HMOX1) to promote ferroptosis.

2. Materials and methods

2.1. Reagent

Docetaxel, Cisplatin, Adriamycin, and Gemcitabine were purchased from the Second Hospital of Shandong University (Jinan, China). Putrescine (Put), spermidine (Spd), spermine (Spm), glutathione (GSH), and difluoromethylornithine (DFMO) were obtained from Aladdin Biochemical Technology (Shanghai, China). Erastin, ferrostatin-1 (Fer-1), necrostatin-1 (Nec-1), acetylcysteine (NAC), and MG132 were obtained from Selleck Chemicals (Houston, TX, USA). Deferoxamine (DFO), mitoquinone mesylate (MitoQ), RSL3, GC7 Sulfate (GC7), tetrathiomolybdate (TTM), hydroxychloroquine (HCQ) and cycloheximide (CHX) were purchased from MedChemExpress (Shanghai, China). Z-VAD-FMK was obtained from Beyotime (Shanghai, China).

2.2. Cell culture

PC3, A549, H1299, H292, K562, HepG2, EC109, HCT116, A2780, and A2780/CDDP (Cisplatin-resistant cell line derived from A2780) were purchased from American Type Culture Collection (ATCC, Manassas, VA, USA). DU145, H460, H460/RT (paclitaxel-resistant cell line derived from H460), SW620, H1688, and H446 were purchased from the Shanghai Cell Bank of the Chinese Academy of Sciences (Shanghai, China). Human prostate cancer cells PC3, DU145, human lung carcinoma H460, H460/Tax, A549, H1688, H446, H292, H1299, human esophageal cancer EC019 cells, human ovary cancer A2780, A2780/CDDP cells and colon cancer LOVO and HCT116 cells were cultured in RPMI-1640 media with 10% FBS, 100 U/mL penicillin, and 100 μg/mL streptomycin. Liver cancer HepG2 and Colon cancer SW620 cells were cultured in DMEM media with 10% FBS and antibiotics. All these cells were incubated at 37 °C in a 5% CO_2 humidified incubator.

2.3. Cell viability

Cells were seeded into 96-well plates at an initial density of 1×10^4 cells/well and incubated at 37 °C overnight. Then the cells

were treated with compounds or DMSO (served as the control) for 24 h. Cell viability was determined by 3-(4,5-dimethylthiazol-2-yl)-2,5-diphenyltetrazolium (MTT, Olarbio Science & Technology, Beijing, China) assay performed at least 3 replicates for each concentration.

2.4. Measurement of lipid ROS

The level of lipid ROS was detected by C11-BODIPY 581/591 (Thermo Scientific, Shanghai, China). Cells were seeded at appropriate density in a six-well and exposed to the indicated treatments, then 5 μmol/L of C11-BODIPY 581/591 dye was added and incubated at 37 °C in the dark for 30 min. The fluorescence intensity was measured using flow cytometry.

2.5. Malondialdehyde (MDA) assay

The MDA levels in tumor cells or tissues were measured using a Lipid Peroxidation MDA Assay Kit (Nanjing Jiancheng, Nanjing, China) according to the manufacturer's instructions. The cells were seeded in a 100 mm cell culture dish and treated with the indicated reagents for 12 h. Then the cells were divided into two equal parts after collection, in which one part was used for protein concentration determination and the other part was detected for intracellular MDA. The tissues were treated with 0.86% saline and homogenized by an ultrasonic cell disruptor. The 10% homogenate was centrifuged at a speed of 12,000 rpm using a centrifuge for 10 min, then the supernatant was collected for measuring MDA levels and protein concentration. MDA levels were normalized to the total amount of protein in cells or tissues.

2.6. Ferrous iron assay

The Fe^{2+} levels of cells were detected by FerroOrange dye (Dojindo Laboratories, Kumamoto, Japan). Cells were exposed to the indicated treatments for 8 h. After treatment, FerroOrange was added to the cells incubated at 37 °C for 30 min. The Fe^{2+} levels of cells were acquired using flow cytometry. The Fe^{2+} levels of tissues were measured using the Ferrous Ion Content Assay Kit (Olarbio Science & Technology) according to the manufacturer's instructions. The 10% homogenate of tissue was centrifuged and the supernatant was collected for measuring Fe^{2+} levels. Fe^{2+} levels were normalized to the total amount of protein in tissues.

2.7. Glutathione (GSH) assay

Intracellular GSH levels were determined using a GSH Assay Kit (Nanjing Jiancheng). Cells were seeded in a 100 mm cell culture dish and treated with the indicated reagents for 12 h. Then, the subsequent procedures were performed according to the manufacturer's instructions. The data were detected by a microplate reader.

2.8. Measurement of intracellular ROS

The levels of intracellular ROS were detected by a 2′,7′-dichlorofluorescin diacetate (DCFH-DA) assay kit (Beyotime). The cells were seeded in 6-well plates and suspended in 1 mL of 10 μmol/L DCFH-DA for 20 min at 37 °C in the dark after being treated with the indicated reagents for 8 h. The cells were washed twice with PBS and the fluorescence intensity was detected by flow cytometry.

2.9. Measurement of mitochondrial membrane potential (MMP) and ATP

MMP was measured by a JC-1 assay kit (Beyotime) according to the manufacturer's instructions. The cells were seeded in 6-well plates and treated with the indicated reagents. After treatment, the cells were stained with JC-1 for 20 min at 37 °C, the results were observed by the fluorescence microscope and flow cytometry. MMP was analyzed by the ratio of red/green fluorescence intensity using FlowJo software. Intracellular ATP levels were determined using an Enhanced ATP Assay Kit (Beyotime) according to the manufacturer's instructions. After treatment with indicated reagents for 8 h, cells were washed and cell lysates were centrifuged at 12,000 × *g* at 4 °C for 5 min, the supernatant was collected to measure chemiluminescence with a luminometer plate reader. Intracellular ATP levels were normalized to the amount of protein in cells.

2.10. Real-time quantitative PCR analysis (RT-qPCR)

The total RNA was extracted from cultured cells and tissues using a TRIzol reagent (TaKaRa, Japan) following the manufacturer's instructions. Reverse transcriptase reactions were performed using the ReverTra Ace qPCR RT Kit (TOYOBO, Japan). RT-qPCR of cDNA was performed with SYBR Green reaction master mix (TOYOBO) on a QuantStudio™ 5 system (Thermo Fisher). Target gene mRNA expressions were normalized to the level of β-actin expression. Changes in transcript level were calculated using $2^{-\Delta\Delta Ct}$ method. The primers are listed in Supporting Information Table S1.

2.11. Western blot analysis and immunoprecipitation

Cells and tissues were washed with ice-cold phosphate-buffered saline (PBS) and ice-cold RIPA buffer containing protease inhibitors and phosphatase inhibitors (Invitrogen). Protein concentrations were quantified by BCA protein assay (Beyotime). Proteins were separated using SDS-PAGE gel and transferred to NC membranes. After being blocked in 5% skim milk at room temperature for 1 h, the membranes were incubated overnight at 4 °C with primary antibodies before being probed with the appropriate peroxide-conjugated secondary antibodies. The blots were visualized based on an enhanced chemiluminescence (ECL) method. For immunoprecipitation, cell lysates were pre-cleared with protein A/G Plus-Agarose beads (Santa Cruz), and then incubated with anti-Myc at 4 °C overnight. The immunocomplexes were captured by the addition of 20 μL protein A/G Plus-Agarose beads, and washed with RIPA buffer. The beads were heated at 95 °C for 5 min in loading buffer before immunoblotting assays. The detailed antibody information is included in Supporting Information Table S2. The relative protein expression analysis was performed using ImageJ software.

2.12. RNA-sequencing (RNA-seq) analysis

PC3 Cells were treated with indicated reagents for 8 h and three replicates for each group were collected. Total RNAs were extracted from cells using TRIzol reagent. RNA sequencing and data analysis were performed by Lc-bio Technologies (Hangzhou, China). Differentially expressed genes between groups were analyzed by R package edgeR according to the criteria with corrected *P* values of 0.05 and absolute fold-changes of 2.

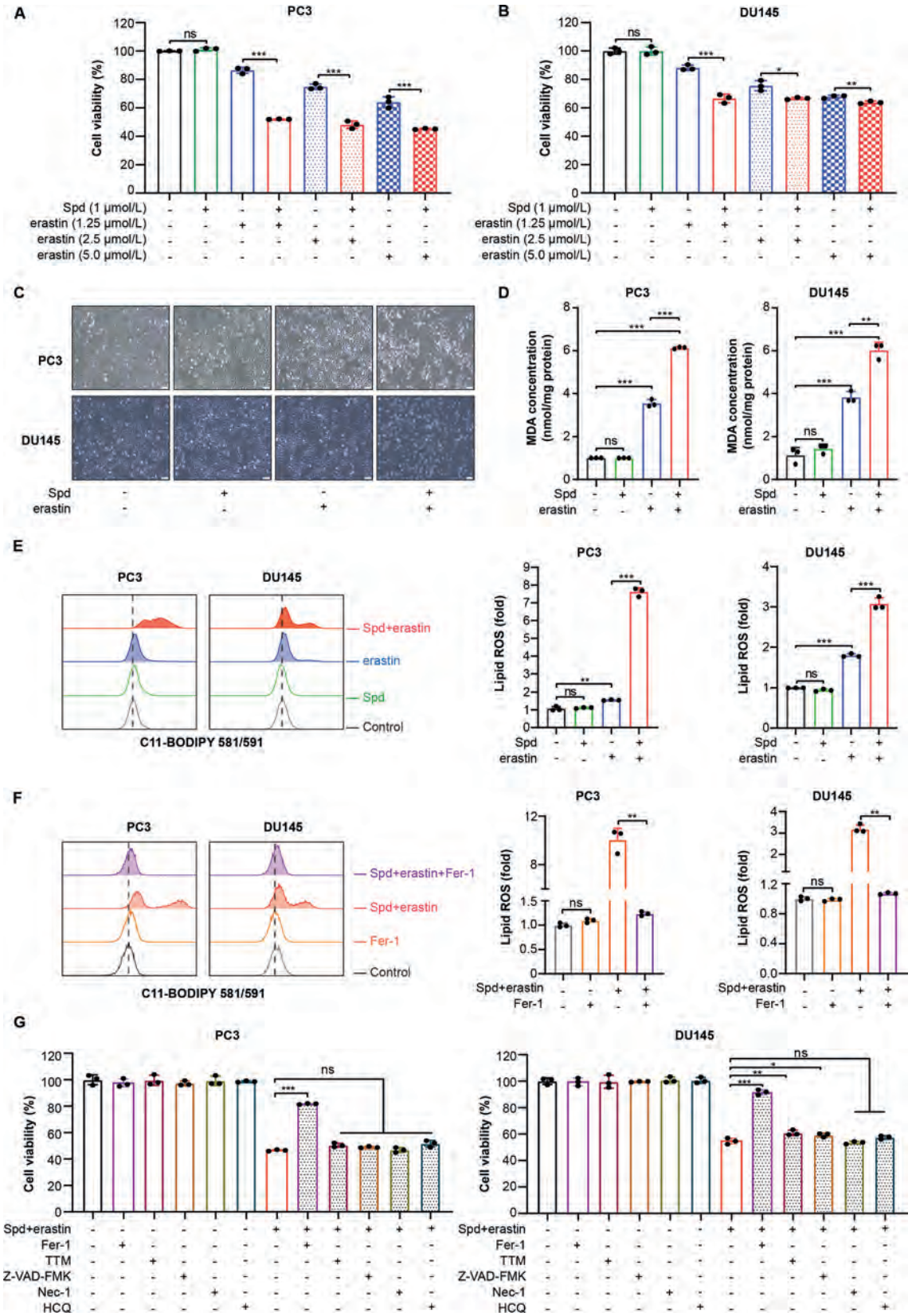

Figure 1 Spd synergistically sensitized erastin-induced ferroptosis in prostate cancer cells. (A, B) PC3 and DU145 cells were treated with Spd (1 μmol/L) and different concentrations of erastin (1.25, 2.5, and 5 μmol/L) for 24 h. The cell viability was measured by MTT assay ($n = 3$). (C) Representative phase-contrast microscopic images of PC3 and DU145 cells after being treated with DMSO, Spd (1 μmol/L), erastin (1.25 μmol/L), or their combination for 24 h. Scale bar, 100 μm. (D) The MDA levels of PC3 and DU145 cells were detected by the MDA assay kit

2.13. Transient transfection of plasmids and siRNAs

For RNA interference, siRNA duplex oligonucleotides or scramble oligonucleotides were synthesized from GenePharma (Shanghai, China). The plasmids containing pcDNA3.1-Myc-NRF2 and pcDNA3.1-HA-Ub were purchased from ViGene Biosciences (Jinan, China). PC3 Cells were transfected using Lipofectamine 2000 (Invitrogen Life Technologies, Carlsbad, CA, USA) according to the manufacturer's instructions. Small interference sequences of HMOX1 and NRF2 have been used and verified in other reports[12]. The siRNA sequences are provided in Supporting Information Table S3.

2.14. Proteasome activity assay

The proteasome trypsin-like (Try-L) activity was measured by the proteasome substrates Bz-VGR-AMC (Enzo Life Sciences, USA). The cells were seeded in 6-well plates and treated with the indicated reagents. Then the whole cell lysates were prepared with lysis buffer (50 mmol/L Tris−HCl pH 8.0, 150 mmol/L NaCl, 5 mmol/L EDTA, 0.5% NP40, 2 mmol/L DTT) for 30 min. 20 μg of cell lysates were incubated with Bz-VGR-AMC for 30 min at 37 °C in the dark. The results were observed by the fluorescence microplate reader. The fresh tissues were collected and treated with proteasome activity assay lysis buffer, and then the 10% homogenate was centrifuged at a speed of 12,000 rpm using a centrifuge for 10 min at 4 °C, the 30 μg of supernatant was collected for measuring proteasome activity.

2.15. Molecular docking analysis

To explore the binding site and the binding effect of Spd with proteasome subunits, AutoDock[13], molecular modeling simulation software for protein-ligand docking, was used. The structures of the PSME3 (PDB ID: 7YQD[14]) and PSME4 (PDB ID: 6KWY[15]) were obtained from the Protein Data Bank[16]. We conducted docking studies with the flexible ligand (spermidine) and the rigid receptor (PSME3 and PSME4). The three-dimensional coordinates of the drug molecules were downloaded from the Drug Bank database[17].

A Lamarckian genetic algorithm (LGA)[18,19] was used for generating binding poses. The docking was initiated with 150 randomly positioned poses, a maximum of 2.7×10^7 generations, and a maximum number of 2.5×10^7 energy evaluations. The rate of gene mutation, rate of crossover, and elitism parameters were set as 0.02, 0.80, and 1, respectively. For each PSME3 or PSME4-spermidine docking, 30 docked poses were generated. The best binding energy conformation was selected to be analyzed further. The PyMOL package was used to visualize the binding interactions between these ligands and a 3D model of PSME3 or PSME4.

2.16. Tumor xenograft experiment

Male BALB/c nude mice (5 weeks of age) were obtained from Jiangsu Huachuang Xinuo Pharmaceutical Technology Co., Ltd. (Taizhou, China). After a week of acclimatization, PC3 cells (5×10^6 cells) were suspended in 200 μL saline and injected subcutaneously in the right anterior flanks of the mice. Tumors were measured with calipers every other day. For antitumor efficiency of Spd and erastin combined therapy *in vivo*, when tumors reached 50−100 mm^3, the mice were randomized into 7 groups ($n = 6$ for each group): 1) Placebo group (5% DMSO, 40% PEG 400, 5% Tween 80 and sterile water); 2) Spd group (10 mg/kg Spd dissolved in saline)[20,21]; 3) Put group (10 mg/kg Put dissolved in saline); 4) High-dose erastin group (15 mg/kg erastin dissolved in 5% DMSO, 40% PEG 400, 5% Tween 80 and sterile water); 5) Low-dose erastin group (5 mg/kg erastin); 6) Spd + erastin group (10 mg/kg Spd + 5 mg/kg erastin); 7) Put + erastin group (10 mg/kg Put+ 5 mg/kg erastin). For the effect of GC7 on the combination therapy in mouse tumor models, when tumors reached 50−100 mm^3, the mice were assigned randomly into 4 treatment groups ($n = 5$ for each group): 1) Placebo group (5% DMSO, 40% PEG 400, 5% Tween 80 and sterile water); 2) GC7 group (2 mg/kg GC7 dissolved in saline)[22]; 3) Spd + erastin group (10 mg/kg Spd + 5 mg/kg erastin); 4) GC7 + Spd + erastin group (2 mg/kg GC7 + 10 mg/kg Spd + 5 mg/kg erastin). All the groups were administered by intraperitoneal injection daily. The mice's weight and tumor volume were measured every other day. Tumor volumes (mm^3) were calculated according to Eq. (1):

$$\text{Tumor volumes } (mm^3) = 0.5 \times L \times W^2 \quad (1)$$

where L is length and W is width. After 14 days of treatment, all mice were sacrificed and tumors were removed and weighed. All animal experiments were approved by the Ethics Committee of the School of Medicine of Shandong University (Jinan, China). The research was conducted following the National Institutes of Health Guide for Care and Use of Laboratory Animals (NIH Publication No. 8023, revised in 1978).

2.17. Hematoxylin and eosin (H&E) staining and immunohistochemistry (IHC)

Xenograft tumor tissue was fixed with 4% paraformaldehyde and embedded with paraffin using an embedding machine (Sakura, Japan). Paraffin-embedded tumor specimens were sectioned at a 5 μm thickness for H&E staining and immunohistochemical analysis. H&E staining was performed using routine methods. For immunohistochemical analysis, the slides were stained with Ki67, HMOX1, and NRF2 overnight at 4 °C. After antigen retrieval, the slides were stained with IgG-conjugated HRP and DAB (Vector Laboratories), and samples were counterstained with hematoxylin and subjected to capture images by Nanozoomer Digital Pathology scanner microscopy (NanoZoomer S60).

2.18. Measurement of polyamines

Polyamines from treated cells were isolated, benzoylated, and analyzed by HPLC as previously described[23]. Briefly, 10^7 cells

($n = 3$). (E) The lipid ROS levels of PC3 and DU145 cells were detected with C11-BODIPY 581/591 after being treated with DMSO, Spd (1 μmol/L), erastin (1.25 μmol/L), or their combination for 8 h ($n = 3$). (F) The lipid ROS levels of PC3 and DU145 cells were observed with the treatment of Spd and erastin with or without ferroptosis inhibitor (Fer-1, 1 μmol/L) ($n = 3$). (G) PC3 and DU145 cells were pretreated with Fer-1 (1 μmol/L), Z-VAD-FMK (5 μmol/L), Nec-1 (1 μmol/L), CHQ (10 μmol/L) and TTM (1 μmol/L) for 2 h, and then cells were added with Spd and erastin as single agents or combinations for an additional 24 h. The cell viability was measured by MTT assay ($n = 3$). Data are shown as mean ± SD. Significance was analyzed with Student's t test. *$P < 0.05$; **$P < 0.01$; ***$P < 0.001$; ns, not significant.

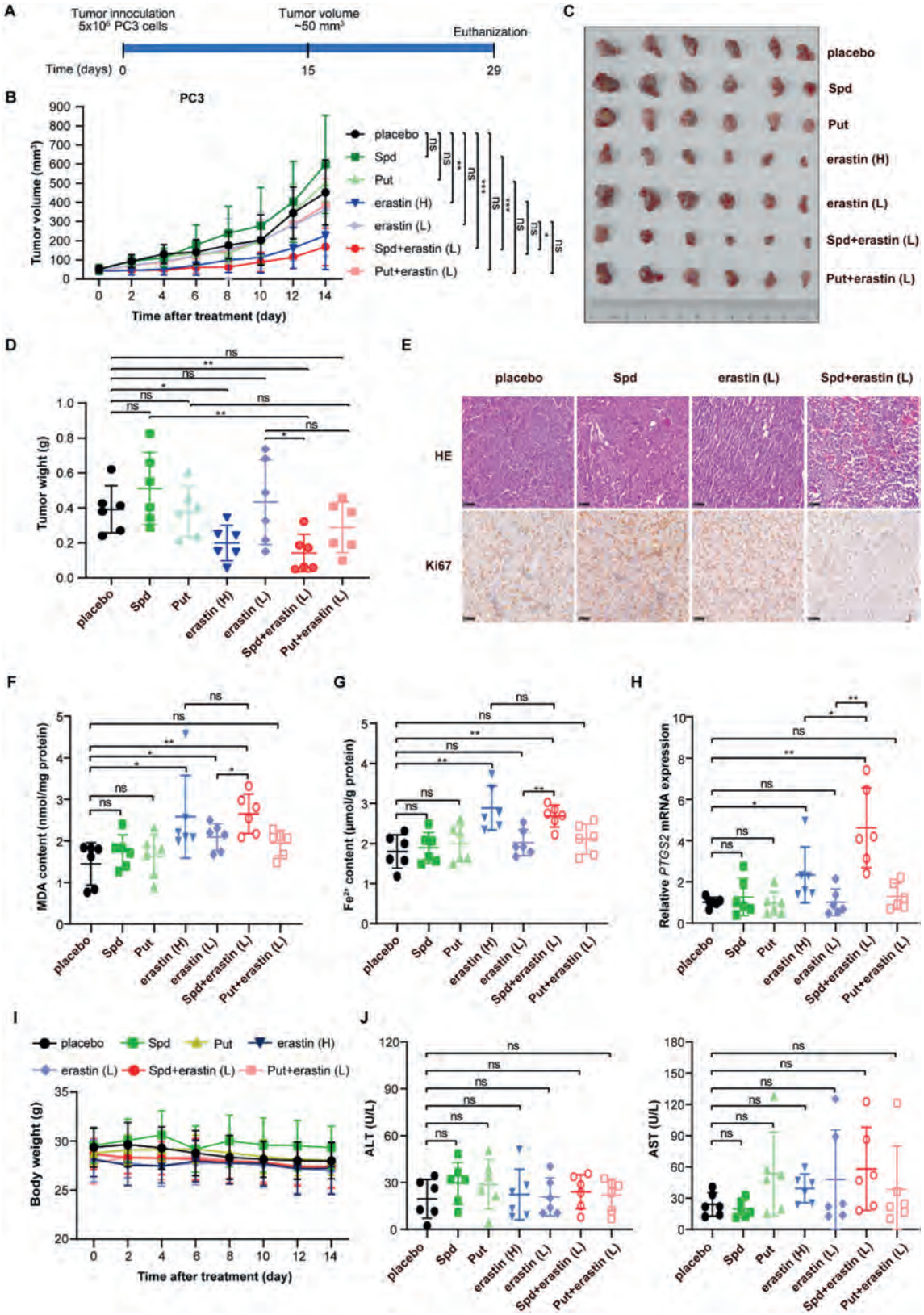

Figure 2 Spd combined with erastin exerted a potential anti-tumor activity *in vivo*. (A) Schematic overview for the administration in a nude mice model. (B) When tumors reached 50−100 mm^3, the mice were assigned randomly into 7 treatment groups and treated with placebo, 10 mg/kg Put, 10 mg/kg Spd, 15 mg/kg erastin, 5 mg/kg erastin, 10 mg/kg Spd + 5 mg/kg erastin and 10 mg/kg Put + 5 mg/kg erastin, respectively. Tumor volumes of PC3 xenografts were monitored every other day ($n = 6$). (C) Representative images mages of isolated tumors from different groups. (D) Tumor weights in 7 groups ($n = 6$). (E) The H&E staining and the Ki67 immunohistochemical staining of the tumors.

were collected and resuspended the cells in 1 mL PBS. Polyamines from cells were extracted and protonated by adding 100 μL of 50% (*w*/*v*) trichloroacetic acid solution with 20 μL (20 nmol) of the 1,8-diaminooctane internal standard to each tube. 500 μL of TCA cell extract was added to 2 mL of 2 mol/L NaOH to benzoylation with 7 μL of benzoyl chloride solution at 40 °C for 20 min. Then the reaction was stopped by using 2 mL of saturated NaCl solution. The benzoylated polyamine derivatives were extracted with 2 mL ethyl acetate. The benzoylated polyamine derivatives were analyzed using an Agilent 1260 HPLC with an Agilent Zorbax SB-C18 column (5 μm, 250 mm × 4.6 mm). Using the relative molar response derived from benzoylated polyamine derivatives and 1,8-diaminooctane standards, the amount of benzoylated polyamine derivatives was calculated and normalized to the total sample protein.

2.19. Statistical analysis

Experiments were replicated thrice. Data were analyzed with GraphPad Prism 9.0 (GraphPad Software Inc., USA). Statistical analysis was performed with the *t*-test for two groups or one-way ANOVA for multiple groups. Values were expressed as mean ± standard deviation (SD). Statistical significance in all experiments was considered at P values < 0.05.

3. Results

3.1. Spd supplement facilitates ferroptosis in prostate cancer cells

We initially examined the polyamine levels to test whether they affect DFMO in a panel of cancer cells. The results showed that the levels of Spd and Spm were higher than that of Put in the cancer cells tested. It appeared that the IC_{50} values of DFMO were marginally associated with the polyamine amount (Supporting Information Fig. S1A and S1B). Cells were exposed to Put, Spd, and Spm with different concentrations to determine whether the supplement of polyamines has an impact on cell survival. The results indicated that polyamines at 1 μmol/L had no detectable effect on cell viability, but exerted inhibition on cell viability at higher concentrations (Fig. S1C). Therefore, we selected polyamines (1 μmol/L) to test whether polyamines influence the cytotoxic effect of chemotherapeutics used in the clinic. As shown in Fig. S1D, cell viability was not influenced when cells were exposed to low concentrations of the polyamines combined with docetaxel, cisplatin, adriamycin, and gemcitabine, however, cell survival was significantly suppressed when co-treatment of Spd with the ferroptosis inducer erastin, an inhibitor of solute carrier family 7 member 11 (SLC7A11), in prostate cancer PC3, DU145, and the colorectal cancer SW620 cells, suggesting that polyamines may increase the sensitivity of these cells to ferroptosis induction.

To validate the influences of Spd in ferroptosis, we treated PC3 and DU145 cells with different combinations of erastin to monitor the change in cell viability. The results clearly showed that Spd significantly reduced cell viability when combined with erastin at low concentrations over 12 h (Fig. 1A−C, Fig. S1E and S1F). Analysis of ferroptosis parameters indicated that cotreatment with Spd and erastin predominantly increased intracellular malondialdehyde (MDA) levels and lipid ROS production (Fig. 1D and E), which are two classical features of ferroptosis. The production of lipid ROS induced by the combination treatment was significantly abolished in the presence of ferroptosis inhibitor ferrostatin-1 (Fer-1) (Fig. 1F), supporting the observations that Spd synergistically enhanced erastin-induced ferroptosis. Furthermore, the apoptosis inhibitor Z-VAD-FMK, the necroptosis inhibitor necrostatin-1 (Nec-1), the cuproptosis inhibitor tetrathiomolybdate (TTM), and the autophagy inhibitor hydroxychloroquine (HCQ) had limited ability to restore the cell death by Spd and erastin, providing evidence that Spd exacerbated ferroptosis induced by erastin (Fig. 1G). The effect of Spd on ferroptosis was further confirmed using RSL3, another ferroptosis inducer targeting glutathione peroxidase 4 (GPX4) (Supporting Information Fig. S2). Taken together, these results demonstrate that Spd significantly sensitized ferroptosis in prostate cancer cells.

3.2. Spd promotes anti-tumor efficacy of erastin in mice

To evaluate the anti-tumor potential of Spd, a xenograft model was established in nude mice for this purpose (Fig. 2A). Animals treated with placebo, Spd and Put alone, erastin with different doses (high, 15 mg/kg; low, 5 mg/kg), or Spd and Put plus erastin (5 mg/kg), respectively. The results revealed that Spd, but not Put, marginally increased tumor growth, although this increase in tumor volume and weight failed to be statistically significant (Fig. 2B−D). In the case of erastin, a high dose of erastin (H) drastically exerted inhibition on tumor growth, while erastin at a low concentration (L) combined with Spd led to a predominant decrease in tumor growth as indicated by the reduction in tumor volume/weight and Ki67 positive staining, which was not significantly displayed in mice exposed to Put combined with erastin (Fig. 2B−E and Supporting Information Fig. S3A). Further analysis indicated that MDA and Fe^{2+} levels significantly increased in the tumor samples from mice treated with erastin (H) alone or Spd combined with erastin (L), whereas Spd, Put, or Put plus erastin (L) had limited effect on these two parameters (Fig. 2F and G). As a downstream marker of ferroptosis, prostaglandin G/H synthase 2 (PTGS2) mRNA expression was significantly upregulated in mice treated with erastin (H), or Spd combined with erastin (L), but not in other groups (Fig. 2H). Moreover, combination treatment with Spd and erastin displayed no measurable toxicity as evidenced by the changes in animal body weight and the release of aspartate transaminase (AST) and glutamic pyruvic transaminase (ALT) in the blood, two indicators of liver damage (Fig. 2I and J). In a macroscopic analysis, The H&E staining of major organs showed that there were no appreciable abnormalities or noticeable organ damage in the combination group (Fig. S3B). Thus, Spd combined with erastin exerts a potential anti-tumor activity with little toxicity.

Scale bar, 50 μm. (F) The relative MDA levels in different groups were measured by the MDA kit ($n = 6$). (G) The levels of Fe^{2+} concentrations were detected in isolated tumors by the Ferrous Ion Content Assay Kit ($n = 6$). (H) The *PTGS2* mRNA expressions of isolated tumors were detected ($n = 6$). (I) Body weights of mice ($n = 6$). (J) Biochemical analysis of liver aspartate transaminase (AST) and glutamic-pyruvic transaminase (ALT) ($n = 6$). Data are shown as mean ± SD. Significance was analyzed with Student's *t* test. $^{*}P < 0.05$; $^{**}P < 0.01$; $^{***}P < 0.001$; ns, not significant.

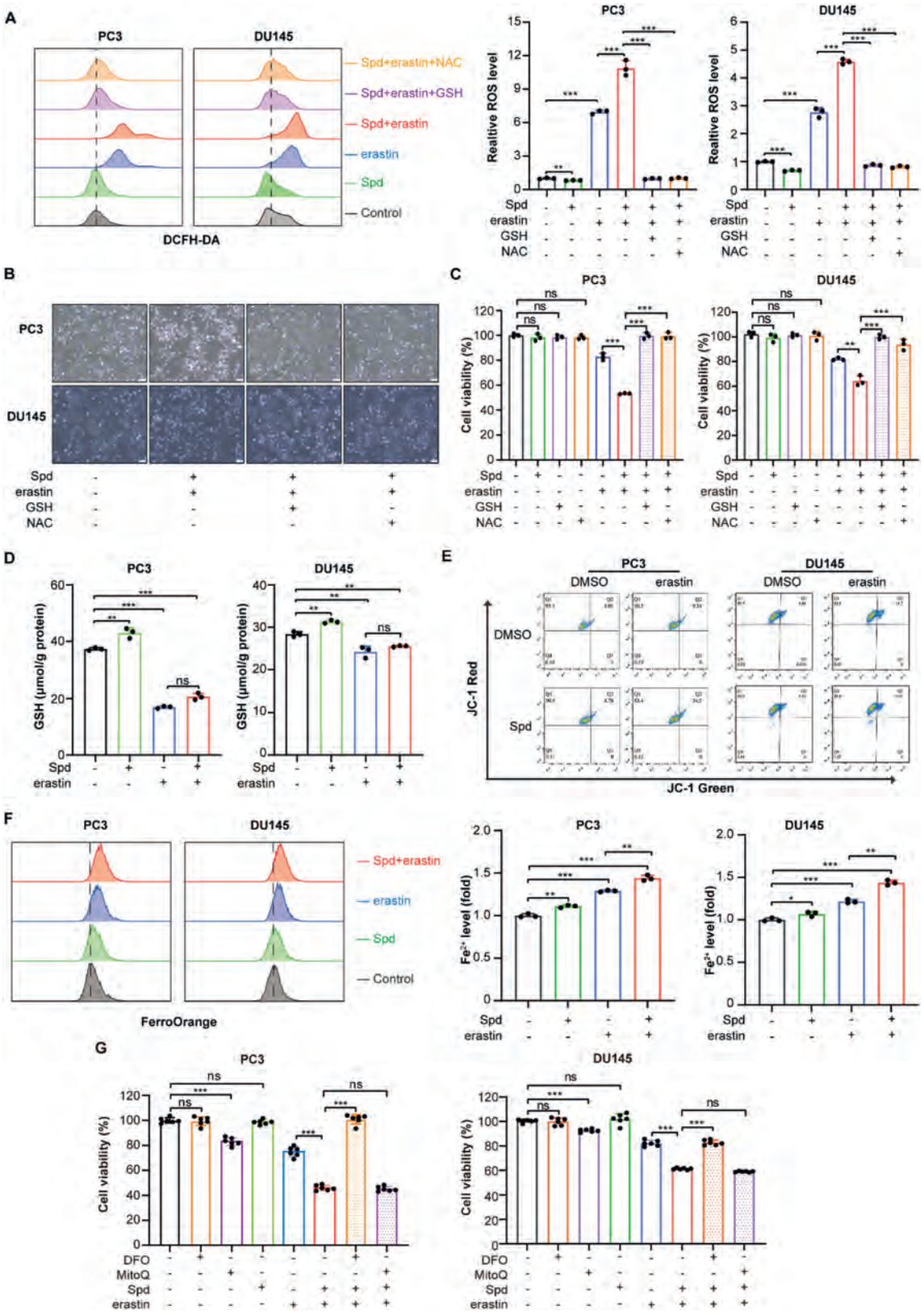

Figure 3 Spd sensitized ferroptosis through a ROS-dependent mechanism that is associated with the accumulation of iron. (A) PC3 and DU145 cells were treated with Spd and/or erastin in the presence or absence of ROS scavengers GSH (0.5 mmol/L) or NAC (0.5 mmol/L) for 8 h, and the intracellular ROS production was measured by DCFH-DA ($n = 3$). (B, C) PC3 and DU145 cells were pretreated with GSH (0.5 mmol/L) and NAC (0.5 mmol/L) for 2 h, and then cells were added with Spd and erastin as single agents or combinations for an additional 24 h. Representative phase-contrast microscopic images and cell viability were measured ($n = 3$). Scale bar, 100 μm. (D−F) PC3 and DU145 cells

3.3. Spd-sensitized ferroptosis depends on ROS elevation and iron accumulation

Ferroptosis is an excessive reactive oxygen species (ROS)-dependent form of cell death[24], and Spd is closely related to ROS[25], this prompted us to question the change of ROS in response to Spd or Spd plus erastin. Interestingly, Spd itself decreased the intracellular ROS, but promoted ROS production together with erastin (Fig. 3A). Put, the synthetic precursors of Spd, didn't show the effect on ROS production in the presence of erastin (Supporting Information Fig. S4A). Additionally, the promotion of ROS production by Spm, another polyamine derived from Spd, was weaker than that of Spd (Fig. S4A). To assess the role of the effect of ROS in ferroptosis induced by Spd combined erastin, cell viability was monitored with Spd and erastin in the presence of two ROS scavengers glutathione (GSH) and acetylcysteine (NAC). The results demonstrated that GSH and NAC completely suppressed ROS production induced by Spd plus erastin, associated with restoration of cell survival (Fig. 3A−C), highlighting the importance of ROS in Spd-stimulated ferroptosis. As GSH is indispensable to scavenge excessive ROS, the results displayed that Spd, to some extent, increased the intracellular GSH concentration but the intracellular GSH levels didn't increase during the co-treatment with Spd and erastin (Fig. 3D). Mitochondria and Fenton reaction are the major sources of intracellular ROS, we next examined the alteration in mitochondrial membrane potential (MMP) and Fe^{2+} levels. JC-1 staining showed that the MMP did not have a significant change when cells were exposed to Spd and erastin (Fig. 3E). Furthermore, the content of ATP did not further reduce indicating that the combination treatment did not have an additional impact on mitochondrial function (Fig. S4B). Strikingly, Spd remarkedly increased the erastin-induced Fe^{2+} levels, and sustained the Fe^{2+} levels upon cotreatment (Fig. 3F). An iron chelator deferoxamine (DFO) and the mitochondria-targeted antioxidant mitoquinone mesylate (MitoQ) were employed to determine the major sources of intracellular ROS. As shown in Fig. 3G, the cell viability assay revealed that DFO was capable of preventing cell death following Spd and erastin cotreatment, whereas MitoQ was unable to save the cells exposed to cotreatment (Fig. 3G). These results imply that Spd sensitized ferroptosis through a ROS-dependent mechanism that is associated with the accumulation of iron.

3.4. Spd and erastin actives NRF2-HMOX1 signaling

To gain further insights into the Spd-facilitated ferroptosis in prostate cancer cells, we conducted RNA-sequencing (RNA-seq) analysis in PC3 cells treated with Spd alone or combined with erastin. There were 652 differentially expressed genes upon Spd treatment, and the number of 1379 genes were significantly upregulated while 1965 genes were downregulated in the Spd plus erastin treatment (Fig. 4A and Supporting Information Fig. S5A), suggesting the gene profile is dramatically altered upon treatments. The gene set enrichment analysis (GSEA) exhibited high enrichment of upregulated genes involved in proteasome and ferroptosis response to both Spd single and co-treatment (Fig. S5B). Analysis of the 58 genes clustered in the Venn diagram, which were upregulated in cells treated with either Spd or Spd combined with erastin, revealed that they were significantly enriched in the ferroptosis pathway (Fig. 4B−D). Among these genes verified by RT-qPCR assays, we found that the change of heme oxygenase 1 (HMOX1) was most significant, it was predominantly upregulated by Spd, and became more robust when Spd combined with erastin (Fig. 4E). Western blot analysis confirmed the changing pattern of HMOX1 protein in PC3 and DU145 cells treated with Spd alone or Spd combined with erastin (Fig. 4F and Supporting Information Fig. S6A). The down-regulation of the SLC7A11 and GPX4 could promote ferroptosis, but we noticed that SLC7A11 slightly increased, GPX4 remained unchanged in cells challenged with Spd or Spd plus erastin (Fig. 4F and Fig. S6A). Furthermore, elevated HMOX1 was also evidenced in the tumor samples after combination treatments compared to the control group (Fig. 4G−I and J, and Fig. S6B and S6C).

As HMOX1 is regulated by the nuclear factor erythroid 2-related factor2 (NRF2), which is a critical transcriptional factor that responds to oxidative stress to regulate diverse target genes including the heme, iron and GSH metabolism such as HMOX1, ferritin heavy chain (FTH1), ferritin light chain (FTL), glutamate-cysteine ligase regulatory (GCLM) and SLC7A11[26]. We hypothesize that Spd- and erastin-mediated alteration in HOMX1 may be ascribed to the regulatory effect of NRF2. It was displayed that NRF2 was marginally changed in response to Spd, and significantly upregulated upon co-treatment with Spd and erastin (Fig. 4H−J, Fig. S6B−S6D). We subsequently knocked down HMOX1 or NRF2 to examine whether HMOX1 and NRF2 are critical in Spd-mediated combination therapy. The results demonstrated that HMOX1 or NRF2 depletion failed to facilitate cell death induced by Spd combined erastin (Fig. 4K, L and Fig. S6E). Ferritinophagy is a crucial process responsible for regulating the level of Fe^{2+}. Nuclear receptor coactivator 4 (NCOA4) recruits FTH1 to autophagosomes for lysosomal degradation and iron release, triggering ferroptosis[27,28]. We found that the proteins of NCOA4, FTH1 and FTL proteins involved in the regulation of ferritinophagy, were induced creased in the co-treatment (Fig. S6F). Solute carrier family 40 member 1 (SLC40A1/FPN1, a transmembrane exporter of non-heme iron) and transferrin receptor (TFRC, a dimeric glycoprotein receptor for iron-loaded transferrin at the surface of plasma) are the two main iron transporters[29]. However, there was no significant change in the protein levels of TFRC and FPN1 after combination treatment (Fig. S6F). Therefore, it suggested that Spd enhances ferroptosis depending on the up-regulation of NRF2/HMOX1 signaling.

3.5. Spd-mediated EIF5A hypusination promotes NRF2 translation

Given the importance of NRF2 in Spd-stimulated ferroptosis, we sought to explore the mechanism underlying the regulation of Spd

were treated with DMSO, a single or combination of Spd and erastin for 12 h, the GSH levels were analyzed by a GSH Assay Kit (D), the mitochondrial membrane potential was determined by a JC-1 probe (E) and the cellular Fe^{2+} levels were analyzed *via* FerroOrange dye (F), $n = 3$. (G) PC3 and DU145 cells were pretreated with DFO (10 μmol/L) or MitoQ (1 μmol/L) for 6 h, and then cells were added with Spd and erastin as single agents or combinations for an additional 24 h. The cell viability was measured by MTT assays ($n = 6$). Data are shown as mean ± SD. Significance was analyzed with Student's *t* test. $^{*}P < 0.05$; $^{**}P < 0.01$; $^{***}P < 0.001$; ns, not significant.

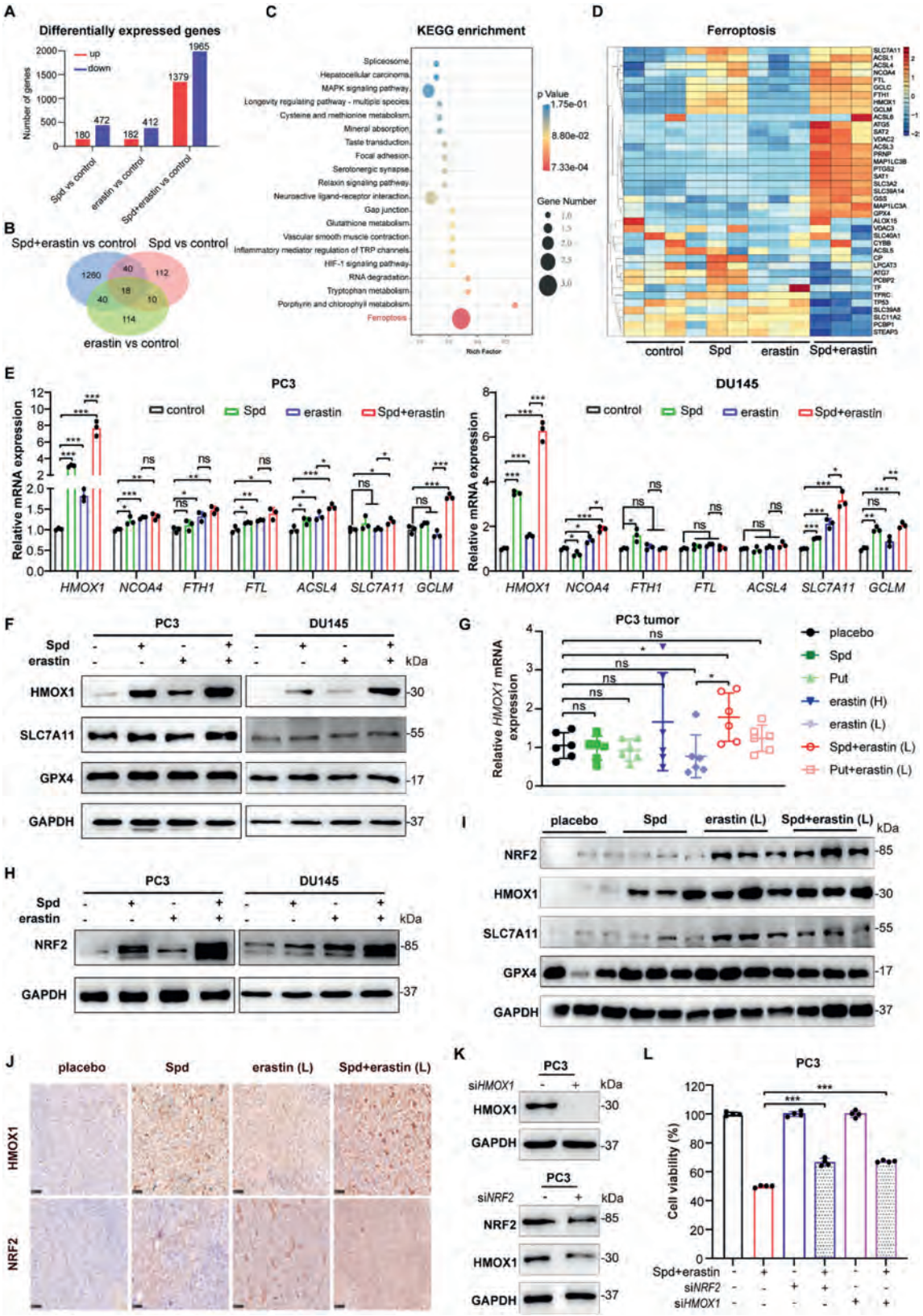

Figure 4 Spd and erastin actives NRF2-HMOX1 signaling pathway. (A) Differentially expressed genes of PC3 cells in response to Spd and erastin as a single or cotreatment measured by RNA-seq ($n = 3$). (B) Venn diagram showed the upregulated genes of PC3 cells at the single or co-treatment. (C) KEGG pathway analysis of genes that were upregulated in cells treated with either Spd or Spd combined with erastin. (D) Heat map analysis showed genes correlated with the ferroptosis pathway ($n = 3$). (E) RT-qPCR analysis of the indicated gene expression associated with the ferroptosis pathway in PC3 and DU145 cells ($n = 3$). (F) Western blot analysis of HMOX1, SLC7A11 and GPX4 in PC3 and DU145 cells

on NRF2. One of the critical functions of Spd is to modify the hypusination of EIF5A (Hyp-EIF5A) that controls the synthesis of target proteins, particularly important for the efficient translation of the N-terminal or long internal polyproline motifs[30] (Fig. 5A). As NRF2 has a triproline motif in its N-terminal end[31,32] (Fig. 5B), we are encouraged to investigate whether EIF5A hypusination affects NRF2 synthesis and attributes to sensitize ferroptosis. The results showed that pretreatment with GC7 Sulfate (GC7), a specific inhibitor of deoxyhypusine synthase (DHPS) that reduces EIF5A hypusination, strongly reversed ferroptosis induced by Spd and erastin (Fig. 5C and D). Enhancement of Hyp-EIF5A by Spd plus erastin was markedly impaired by GC7 treatment, associated with a reduction in NRF2 and HMOX1 (Fig. 5E). Similarly, knockdown of EIF5A attenuated expressions of NRF2 and HMOX1 that were induced by Spd combined with erastin (Fig. 5F). Moreover, as a transcriptional factor, migration of NRF2 (phosphorylated form) into the nucleus was also decreased when EIF5A hypusination was suppressed by DHPS inhibitor GC7 treatment (Fig. 5G), highlighting the importance Spd-triggered EIF5A hypusination in activation of NRF2 expression and function. Additionally, the effects of the GC7 on the combination therapy in mouse tumor models were observed. It was found that treatment with GC7 to inhibit hypusination resulted in a slight reduction of average tumor volume and weight compared to the placebo group, consistent with previous reports (Fig. 5H and I)[22,33-35]. Importantly, GC7 notedly reduced the antitumor effect of combination treatment with Spd and erastin (Fig. 5H and I), supporting the importance of Spd-mediated EIF5A hypusination in ferroptosis induced by erastin. Moreover, Western blot analysis revealed that enhancement of Hyp-EIF5A by Spd plus erastin, accompanied by elevated NRF2, whereas this enhancement by cotreatment was significantly impaired in the presence of GC7 (Fig. 5J and K). These results highlight the regulatory ability of Spd in NRF2, which depends on EIF5A hypusination *in vivo*.

3.6. Spd and erastin suppresses the proteasome activity required for NRF2 degradation

It was noticed that Spd and erastin significantly upregulated the genes enriched in the proteasome system (Fig. S5B), we question whether enhanced proteasomal genes affect NRF2 protein abundance because proteasome-mediated NRF2 degradation is essential for the regulation of its level and function. To confirm the specific regulatory impact of the cotreatment on NRF2 protein, PC3 cells were treated with the protein synthesis inhibitor cycloheximide (CHX) to determine the change of NRF2 protein in a time-dependent manner. A strong increase in the stability and half-life of NRF2 was observed when Spd and erastin were present (Fig. 6A). We then examined the change of Kelch-like ECH-associated protein 1 (KEAP1), which forms part of an E3 ligase response to the regulation of NRF2 ubiquitination by binding to NRF2[36]. It was shown that KEAP1 remained unchanged in response to Spd and erastin treatment (Fig. 6B). However, bulk ubiquitination of proteins was significantly induced in cells exposed to Spd plus erastin (Fig. 6C), importantly, the poly-ubiquitinated NRF2 was noticeably elevated when Spd and erastin were supplemented (Fig. 6C). These results indicated that proteasomal activity was inhibited during the co-treatment. To further validate the proteasome activity in Spd-facilitated cell death, we measured cell survival in the presence of proteasome inhibitor MG132. As shown in Fig. 6D, erastin-induced cell death was further increased when combined with MG132, indicating that inactivation of proteasome augments the inhibitory effect of erastin on cell viability. Of note, MG132 exacerbated the cell death caused by cotreatment with Spd and erastin (Fig. 6D). These motivated us to further investigate the change of proteasome activity when incubated with Spd, erastin, or co-treatment. As shown in Fig. 6E and F, trypsin-like (Try-L) activity, one of the proteases in the proteasome was suppressed in cells and the tumor samples treated with Spd, erastin, or co-treatment (Fig. 6E and F). These observations supported that Spd and erastin had the ability to inhibit proteasome activity.

To elucidate the underlying mechanism(s) by which Spd or co-treatment exhibits suppression of proteasome activity, we validated the change of proteasome-related genes. Consistent with the results of RNA-seq analysis, the mRNA levels of some proteasomal subunits were induced in response to Spd or co-treatment (Fig. 6G and H). Protein abundance of 26S proteasome non-ATPase regulatory subunit 2 (PSMD2), proteasome activator complex subunit 3 (PSME3), 26S proteasome regulatory subunit 4 (PSMC1), and proteasome subunit beta type-7 (PSMB7) slightly increased in PC3 cells, and became more evident in tumor samples after treatments, particularly the co-treatment (Fig. 6I and J). These results suggested that the gene expressions of proteasomal subunits may be feedback-regulated due to proteasome activity being inhibited by Spd and erastin.

Spd is an aliphatic carbon chain including three amine groups, it acts as a polycation active molecule under a physiological environment. This leads us to propose that Spd may interact with proteasomal component(s) to exert inhibitory function rather than to suppress subunit gene expressions. To this end, molecular simulations were conducted and displayed that Spd appears to bind to PSME3 and PSME4, two proteasome activator subunits[37,38]. The docked model (Fig. 6K) showed that the amine group of Spd formed hydrogen bonds or salt bridge with the residues from PMSE3 (Asp54 (A), Glu211 (A), and Glu120 (B)), and the hydrophobic carbon chain of Spd also formed van der Waals forces (mainly hydrophobic interactions) with Leu55 (A), Thr56 (A), Glu120 (B), Lys123 (B), and Pro124 (B) in PSME3 (Fig. 6K−d). As for PSME4, the amine group of Spd formed the hydrogen bond or salt bridge with the residues from Asp1776 and Glu1819 in PSME4 (Fig. 6L). Similar to PSME3, Spd formed van der Waals forces with Glu438, Val1777, Glu1822, and Gln1823 in PSME4 (Fig. 6L−c). Therefore, Spd and erastin suppress proteasome activity, resulting in the accumulation of NRF2 to activate ferroptosis.

($n = 3$). (G) RT-qPCR analysis of *HMOX1* mRNA expression in the harvested tumors ($n = 6$). (H) Western blot analysis of NRF2 in PC3 and DU145 cells ($n = 3$). (I) Western blot analysis of NRF2, HMOX1, SLC7A11 and GPX4 in tumors ($n = 3$). (J) The expressions of HMOX1 and NRF2 in tumor tissues were determined by immunohistochemical staining. Scale bar, 50 μm. (K) The protein levels of HMOX1 and NRF2 were detected in PC3 cells transfected with si*HMOX1* or si*NRF2* ($n = 3$). (L) PC3 cells were transfected with si*HMOX1* or si*NRF2* and then treated with DMSO or Spd plus erastin for 24 h. Cell viability was measured by MTT assays ($n = 4$). Data are shown as mean ± SD. Significance was analyzed with Student's *t* test. $^{*}P < 0.05$; $^{**}P < 0.01$; $^{***}P < 0.001$; ns, not significant.

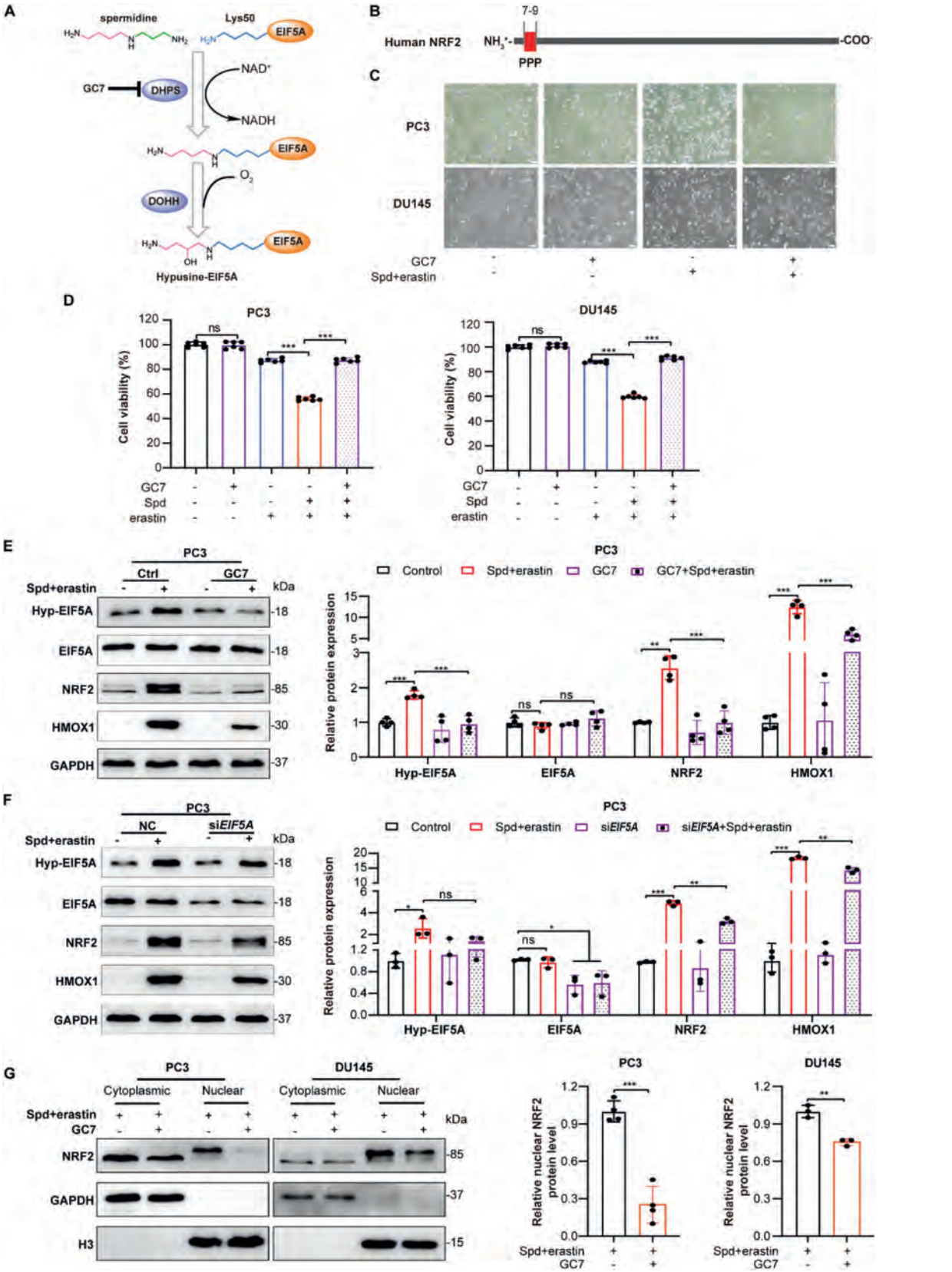

Figure 5 Spd-mediated EIF5A hypusination promotes NRF2 translation. (A) Spermidine is used in EIF5A hypusination pathway in eukaryotes. (B) The triproline motif of Human NRF2. (C, D) PC3 and DU145 cells were pretreated with GC7 (2 μmol/L) for 6 h, and then cells were added with indicated agents for an additional 24 h. Representative phase-contrast microscopic images and cell viability were measured ($n = 6$). Scale bar, 100 μm. (E) Western blot analysis of Hyp-EIF5A, EIF5A, NRF2 and HMOX1 in PC3 cells. Endogenous polyamines of PC3 cells were

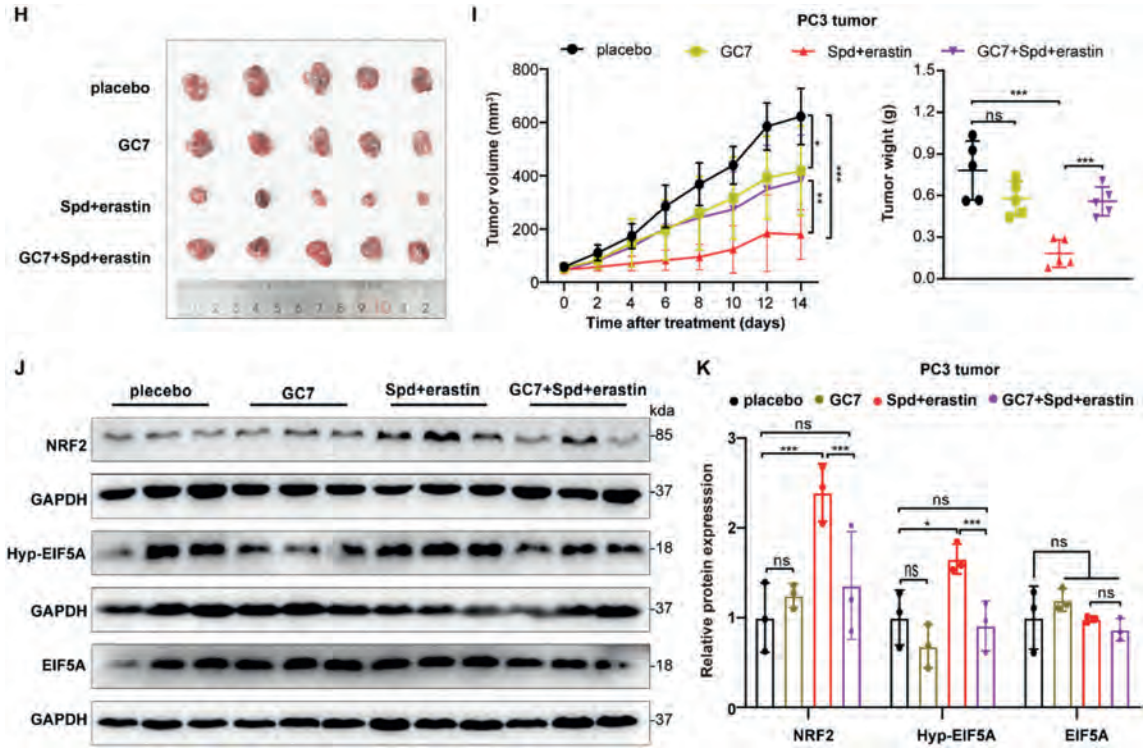

Figure 5 (*continued*).

4. Discussion

This study demonstrates that Spd acts as a stimulator to enhance the anti-tumor efficacy of erastin in prostate cancer. Spd activates NRF2/HMOX1 signaling that results in Fe^{2+} accumulation and ferroptosis induced by erastin. Spd-mediated EIF5A hypusination promotes the translation of the transcription factor NRF2. Meanwhile, Spd and erastin suppress the activity of the proteasome required for NRF2 degradation (Fig. 7).

Polyamines are essential for cell proliferation and growth, the elevated level of polyamines is a defining signature of various types of cancers, thus, the rate-limiting enzyme ODC in the polyamine biosynthetic pathway acts as a therapeutical target in cancer treatment[6]. Interestingly, high levels of preoperative Spd were positively associated with the recurrence of colorectal cancer[39], but supplementation with Spd could reduce the occurrence of colorectal cancer and chemically induced liver cancer[40,41]. The discrepancy between the anti-tumorigenic and tumor growth-promoting functions of Spd might be the role of cell-autonomous *vs* non-autonomous polyamine supply. Regarding the effect of dietary supplementation of Spd on tumor growth, it is believed to be associated with the immune environment and dosage. Our results found that supplementation with Spd (10 mg/kg, i.p., daily) for 14 days to immunodeficient nude mice promoted xenograft growth. Furthermore, a recent study has also observed that singly administered Spm (3 mmol/L, drinking water) for 24 days resulted in a modest enhancement of tumor growth in nude mice[42]. However, a supplement of Spd (2 mmol/L, 100 μL) around the tumor for 14 days could significantly inhibit the growth of colon cells CT-26 and MC38 in mice with normal immune systems[43]. Similarly, Spd did not directly affect tumor growth but enhanced the anti-tumor efficacy of PD-L1 monoclonal antibody and inhibited the tumor growth in mice harboring MC-38 or CT-26 cells, which was achieved intraperitoneally with Spd (2 and 4 mg/kg, respectively) for around 20 days[11]. Moreover, an observational epidemiological study revealed that individuals with a Spd-rich diet are characterized by lower overall mortality and reduced cancer mortality[44]. In this paper, we found that Spd significantly increased the sensitivity of ferroptosis inducers in prostate cancer. We noticed that ferroptosis played a crucial role in the immune response to enhance antitumor immunotherapy[45,46], since chemotherapy of cancers usually allows a certain course of treatment in clinical, and for patients with an immune system, the

depleted by incubating the cells with 1 mmol/L DFMO for 2 days. Polyamine-depleted cells were pretreated with GC7 (2 μmol/L) for 6 h followed by incubating with Spd and erastin for an additional 8 h ($n = 4$). (F) PC3 cells were transfected with si*EIF5A* for 24 h and then incubated the cells with 1 mmol/L DFMO for 2 days. Then cells were treated with Spd and erastin for an additional 8 h. Western blot analysis of Hyp-EIF5A, EIF5A, NRF2 and HMOX1 in PC3 cells were measured ($n = 3$). (G) PC3 and DU145 cells were pretreated with GC7 followed by incubating with Spd and erastin for 8 h. The cytoplasmic/nuclear NRF2 protein expression was assessed using Western blot (PC3, $n = 4$; DU145, $n = 3$). (H) PC3 cells were implanted subcutaneously into nude mice (5×10^6 cells on each flank). When tumors reached 50−100 mm^3, mice were treated i.p. with placebo, 2 mg/kg GC7, 10 mg/kg Spd + 5 mg/kg erastin, or 2 mg/kg GC7 + 10 mg/kg Spd + 5 mg/kg erastin. Representative images of isolated tumors from the end of the experiment ($n = 5$). (I) Tumor volumes of PC3 xenografts were monitored every other day and tumor weights were in 4 groups ($n = 5$). (J) Western blot analysis of NRF2, Hyp-EIF5A and EIF5A in tumors ($n = 3$). (K) Relative protein expression of NRF2, Hyp-EIF5A and EIF5A in tumors ($n = 3$). Data are shown as mean ± SD. Significance was analyzed with Student's *t* test. $^*P < 0.05$; $^{**}P < 0.01$; $^{***}P < 0.001$; ns, not significant.

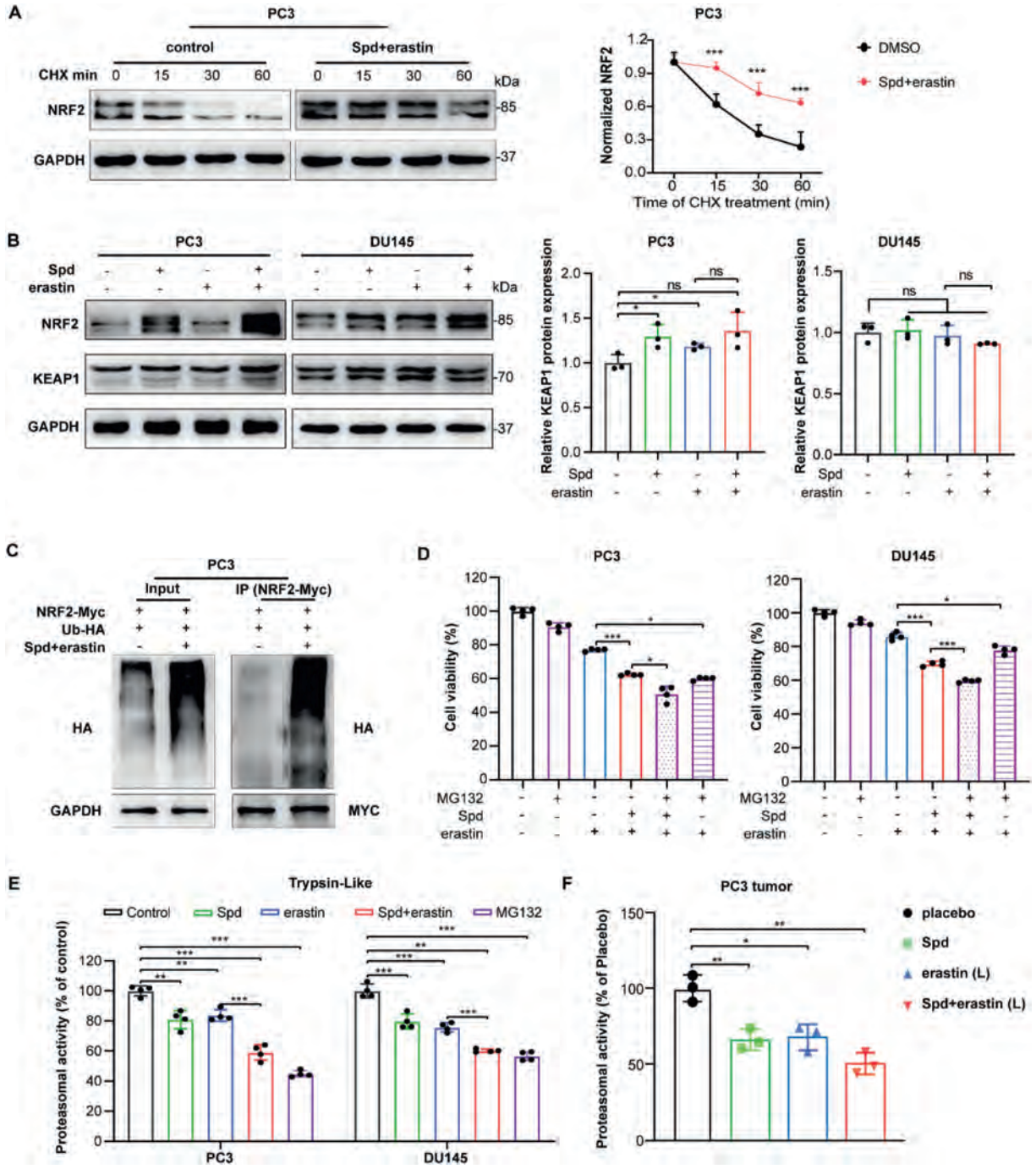

Figure 6 Spd and erastin inhibit the activity of the proteasome. (A) Western blot analysis of NRF2 in PC3 cells treated with CHX (100 μmol/L) for indicated time points (0, 15, 30 and 60 min) after pretreated with PBS or Spd and erastin for 7 h ($n = 3$). (B) Western blot analysis of KEAP1 and NRF2 in PC3 and DU145 cells ($n = 3$). (C) Evaluation of bulk ubiquitination of proteins and polyubiquitinated NRF2 in PC3 cells. PC3 cells transfected with Myc-tagged NRF2 and HA-tagged Ub plasmids for 48 h and treated with Spd and erastin for an additional 8 h ($n = 3$). (D) PC3 and DU145 cells were pretreated with MG132 (20 nmol/L) for 2 h, and then cells were added with indicated agents for an additional 24 h. The cell viability was measured by MTT ($n = 4$). (E) Proteasomal trypsin-like activity in PC3 and DU145 cells treated with indicated agents for 12 h ($n = 4$). (F) Proteasomal trypsin-like activity in PC3 tumor tissues of different groups ($n = 3$). (G) Heat map analysis showed genes correlated with the proteasome pathway ($n = 3$). (H) RT-qPCR analysis of the *PSMB7*, *PSME3*, *PSMD2*, *PSMC1*, and *PSMD1* mRNA expressions in PC3 and DU145 cells ($n = 3$). (I, J) Western blot analysis of PSMD2, PDMC1, PSMB7, and PSME3 protein expressions in PC3 cells and tumor samples ($n = 3$). (K) Molecular modeling of Spd with PSME3. (a) The cryo-electron microscopy (cryo-EM) structure of human PSME3 (PDB ID: 7YQD) displayed as a homo-heptamer. (b) The pocket for ligand docking formed at the interface of the two monomers of PSME3 colored green and yellow respectively. (c) The space-filling-surface view of the docked conformations with the binding energies from −6.40 to −5.50 kcal/mol. (d) The best conformation of Spd with PSME3 and its docked poses. Spd was shown in sticks and the docking score was −6.35. (L) Molecular modeling of Spd with PSME4. (a) The Cryo-EM structure of human PSME4-20S complex (PDB ID: 6KWY). (b) The pocket for

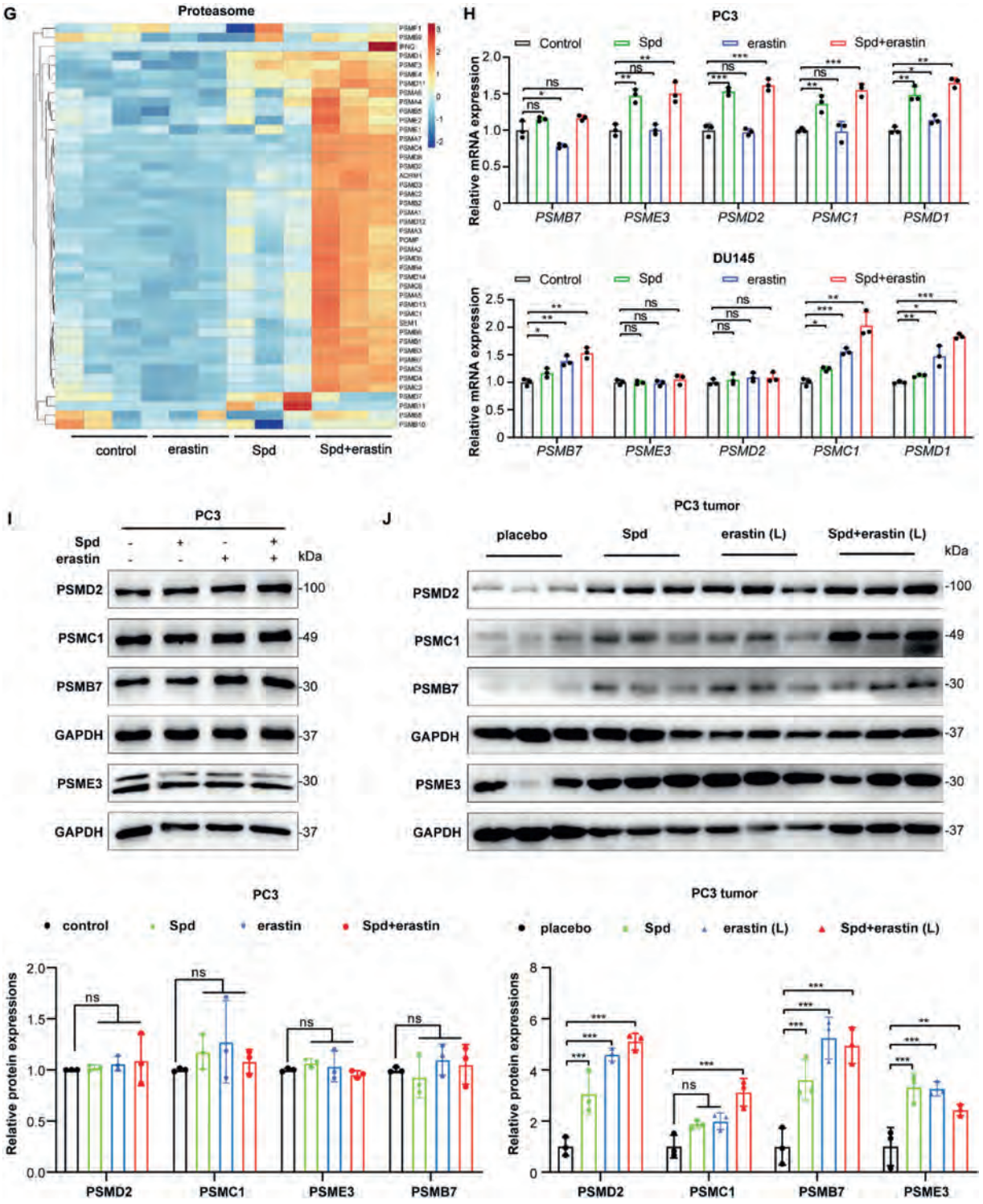

Figure 6 (*continued*).

supplementation with low doses of Spd may significantly enhance the tumor-suppressing capability of ferroptosis inducers in prostate cancer, exerting limited effect on tumor growth while simultaneously augmenting the anti-tumor immune response.

Ferroptosis is a unique form of regulated cell death characterized by redox system imbalance, the lethal accumulation of iron and lipid peroxides, and plays a pivotal role in tumor suppression[47]. System $x^-c-GSH-GPX4$ axis is the major cellular system

ligand docking of PSME4 was circled. (c) The best conformation of Spd with PSME4 and its docked poses. Spd was shown in sticks and the docking score was −5.83. Data are shown as mean ± SD. Significance was analyzed with Student's *t* test. *$P < 0.05$; **$P < 0.01$; ***$P < 0.001$; ns, not significant.

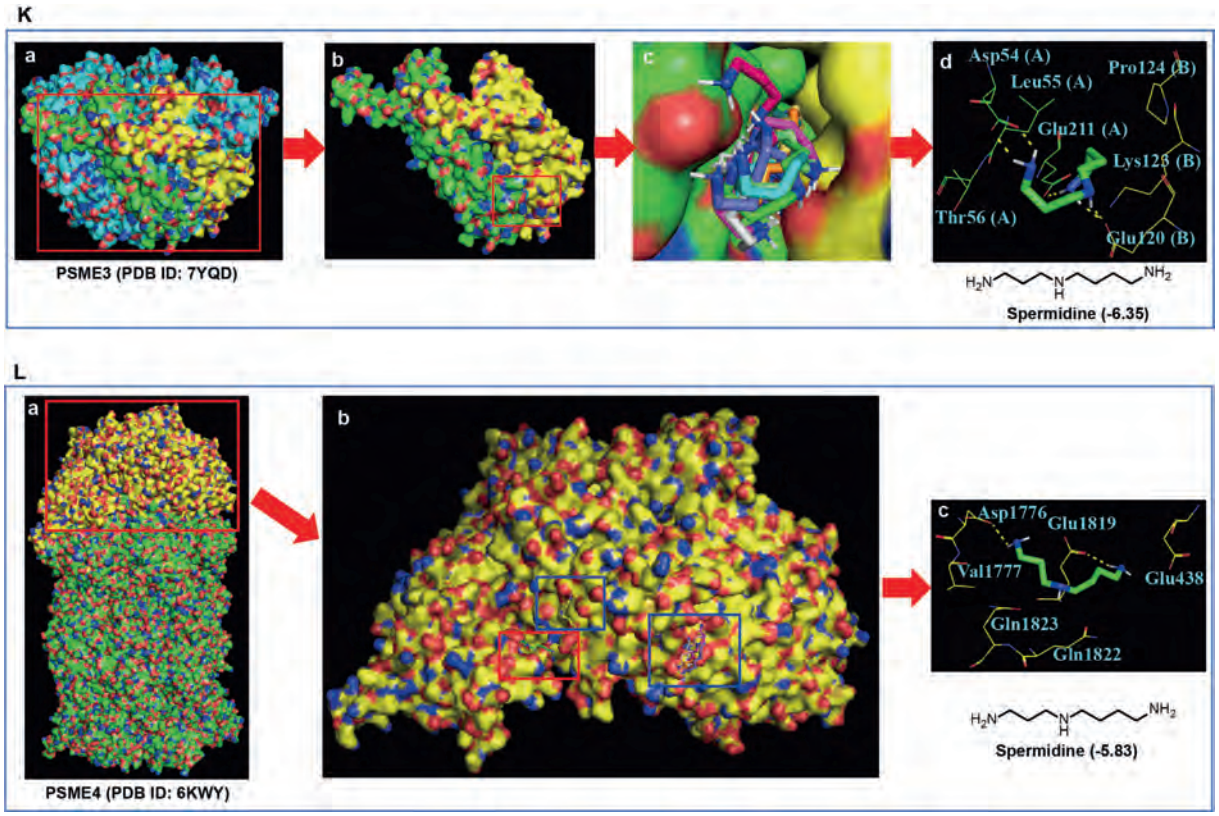

Figure 6 (*continued*).

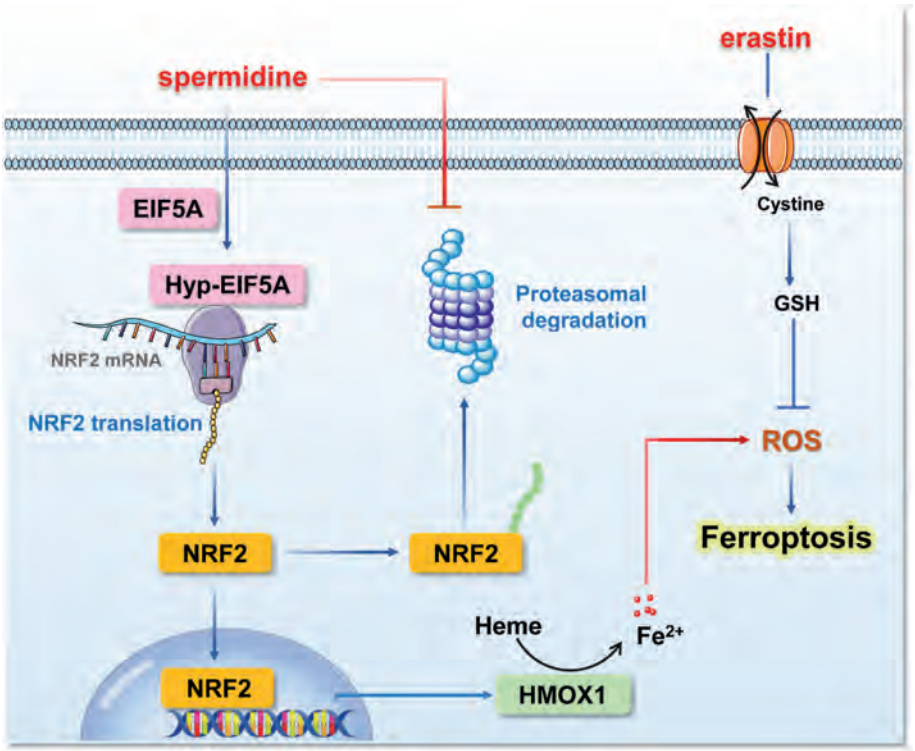

Figure 7 The proposed model for Spd inactivates proteasome activity and enhances ferroptosis in prostate cancer.

in suppressing ferroptosis and maintaining cell survival under oxidative stress conditions[47]. The heavy chain subunit solute carrier family 3 member 2 (SLC3A2), a subunit of system $x^{-}c$, is a critical membrane transporter for polyamine uptake[48,49], suggesting the relationship between polyamines and ferroptosis. 100 μmol/L of Spd can inhibit the proliferation and promote ferroptosis of prostate cancer cell lines by producing ROS *via* amine oxidase copper-containing 1 (AOC1)[50]. As a potent antioxidant, the administration of Spd acts as an anti-ferroptotic effect in many mice models of human disease including Alzheimer's disease, premature ovarian failure, rheumatoid arthritis, and diabetic cardiomyopathy[51-54]. Mechanistically, Spd increases the protein expression of NRF2 to upregulate the system $x^{-}c-GSH-GPX4$ axis, inactivates NCOA4-mediated ferroptinophagy, and decreases p53 and SAT1 expression to attenuate ferroptosis[51-54]. Interestingly, we found that Spd (1 μmol/L) with no influence on the cell viability decreased the intracellular ROS, but promoted ROS production and ferroptosis when combined with erastin in prostate cancer cells. It is demonstrated that anti-ferroptosis proteins, such as SLC7A11 which is highly present in lung cancer A549 cells, contribute to resistance to erastin-induced ferroptosis[55]. However, Spd combined with erastin did not decrease proteins involved in the antioxidant defense system like SLC7A11, GPX4 and NRF2, to some extent, combined treatment resulted in an increase in SLC7A11 expression, and significantly facilitated NRF2 abundance, implicated that enhancement of ferroptosis by Spd plus erastin may be independent on the suppressive effect on SLC7A11 and GPX4. These results may explain why Spd was unable to sensitize A549 cells to erastin because of the highly expressed SLC7A11[55]. Thus, Spd amplifies the Fenton reaction and ROS production to enhance the effect of erastin on ferroptosis, rather than regulating SLC7A11 and GPX4 which are important in conferring erastin resistance. We noted that Spd and erastin significantly also inhibited the growth of colorectal cancer SW620 cells, further investigation is necessary to determine if the combination therapy is an option in colorectal cancer treatment.

It is unclear whether Spd increases NRF2 protein levels to alleviate ferroptosis. Spd is the only substrate of hypusine to promote the maturation of EIF5A, Which is essential for the translation of proteins including TFEB (a protein with one triproline motif), ATG3 (an autophagy-related protein with a tripeptide DDG motif) and MYC (a protein with five distinct pausing motifs)[22,56,57]. We demonstrated that the maturation of EIF5A (Hyp-EIF5A) was crucial for the translation of NRF2. The specific mRNA region that is essential for EIF5A to effectively regulate NRF2 translation requires further elucidation.

Under normal conditions, the binding of NRF2 and KEAP1 leads to the NRF2 degradation by the proteasome[36]. Recent studies have reported that oral administration of Spd stabilizes NRF2 in liver pathologies by activation of microtubule-associated protein 1S (MAP1S), which reduces KEAP1-mediated NRF2 degradation[58]. We found that KEAP1 protein levels remained unchanged in combination with Spd and erastin, but Spd inhibited proteasome activity, leading to an increase in NRF2 protein levels. As a polycation with amine groups, Spd may interact with the proteasomal components PSME3/4, two proteasome activator subunits[37,38], through the formation of salt bonds and hydrophobic interactions. Future studies are required to uncover the structure insights of how Spd binds to PSME3/4.

As endogenous molecules, low doses of polyamines are suggested to have little toxicity as has been demonstrated by several investigations. Dietary supplementation with Spd could help promote healthspan and longevity, and reduce age-related pathologies like hypertension-induced congestive heart failure, cardiac aging, Alzheimer's disease, and female reproductive aging, and is safely tolerated[21,54,59-61]. Moreover, the results in clinical trials including a 3-month (NCT ID: NCT03094546) and a 12-month (NCT ID: NCT02755246) showed that Spd intervention has beneficial effects on inflammation and verbal memory displays excellent safety, tolerability and high compliance rates in Alzheimer's disease[62,63]. Our study also found that the combination of the low dose of Spd with erastin effectively inhibited tumor growth, but did not affect the body weight of mice and showed no significant toxicity in organs including heart, liver, spleen, lung and kidney. Currently, ours and other studies reveal the safety of Spd either in diet or supplement in some disease conditions, suggesting a potential clinical application of Spd and erastin combination therapy in the future, but it requires further and detailed clinical investigations.

5. Conclusions

In conclusion, this work found that Spd promoted erastin-induced ferroptosis in prostate cancer, providing value for targeted polyamines in the treatment of tumors. Since Spd is a safe metabolite found throughout the cell, combining Spd with ferroptosis inducers might be a potentially feasible approach in the treatment of prostate cancer.

Acknowledgments

This work was supported by the National Natural Science Foundation of China (82293682, 82173839, 82373896), GXRC Program of Ji-Nan Science & Technology Bureau (2021GXRC102, China), ECCM Program of Clinical Research Center of Shandong University (2021SDUCRC003, China), and Special Funding for Taishan Scholar Program (tstp20221159, China).

Author contributions

Dan Feng: Writing − original draft, Project administration, Formal analysis, Data curation. Jian Zhang: Software. Huanmin Niu: Methodology, Investigation. Xiaoxue Zheng: Methodology. Mengqi Jia: Supervision. Qiqi Lu: Validation. Jing Wang: Validation. Wenxue Guo: Visualization. Qi Sun: Visualization. Huiqing Yuan: Writing − review & editing, Resources, Project administration, Funding acquisition, Conceptualization. Hongxiang Lou: Resources, Funding acquisition, Conceptualization.

Conflicts of interest

All authors declare that there are no conflicts of interest.

Appendix A. Supporting information

Supporting information to this article can be found online at https://doi.org/10.1016/j.apsb.2025.02.023.

References

1. Vasan N, Baselga J, Hyman DM. A view on drug resistance in cancer. *Nature* 2019;**575**:299−309.

2. Wang X, Zhang HY, Chen XZ. Drug resistance and combating drug resistance in cancer. *Cancer Drug Resist* 2019;**2**:141−60.
3. Mao XM, Wu S, Huang DD, Li C. Complications and comorbidities associated with antineoplastic chemotherapy: rethinking drug design and delivery for anticancer therapy. *Acta Pharm Sin B* 2024;**14**: 2901−26.
4. Cai MP, Song XL, Li XA, Chen M, Guo J, Yang DH, et al. Current therapy and drug resistance in metastatic castration-resistant prostate cancer. *Drug Resist Updat* 2023;**68**:100962.
5. Pegg AE. Functions of polyamines in mammals. *J Biol Chem* 2016; **291**:14904−12.
6. Casero RA, Murray Stewart T, Pegg AE. Polyamine metabolism and cancer: treatments, challenges and opportunities. *Nat Rev Cancer* 2018;**18**:681−95.
7. Arruabarrena Aristorena A, Zabala Letona A, Carracedo A. Oil for the cancer engine: the cross-talk between oncogenic signaling and polyamine metabolism. *Sci Adv* 2018;**4**:eaar2606.
8. Gerner EW, Bruckheimer E, Cohen A. Cancer pharmacoprevention: targeting polyamine metabolism to manage risk factors for colon cancer. *J Biol Chem* 2018;**293**:18770−8.
9. Alexiou GA, Lianos GD, Ragos V, Galani V, Kyritsis AP. Difluoromethylornithine in cancer: new advances. *Future Oncol* 2017;**13**: 809−19.
10. Travers M, Brown SM, Dunworth M, Holbert CE, Wiehagen KR, Bachman KE, et al. DFMO and 5-azacytidine increase M1 macrophages in the tumor microenvironment of murine ovarian cancer. *Cancer Res* 2019;**79**:3445−54.
11. Al-Habsi M, Chamoto K, Matsumoto K, Nomura N, Zhang B, Sugiura Y, et al. Spermidine activates mitochondrial trifunctional protein and improves antitumor immunity in mice. *Science* 2022;**378**: eabj3510.
12. Tang ZM, Ju YH, Dai XC, Ni N, Liu Y, Zhang D, et al. HO-1-mediated ferroptosis as a target for protection against retinal pigment epithelium degeneration. *Redox Biol* 2021;**43**:101971.
13. Morris GM, Huey R, Lindstrom W, Sanner MF, Belew RK, Goodsell DS, et al. AutoDock4 and AutoDockTools4: automated docking with selective receptor flexibility. *J Comput Chem* 2009;**30**:2785−91.
14. Chen DD, Hao J, Shen CH, Deng XM, Yun CH. Atomic resolution Cryo-EM structure of human proteasome activator PA28γ. *Int J Biol Macromol* 2022;**219**:500−7.
15. Guan HX, Wang YW, Yu T, Huang YN, Li MH, Saeed A, et al. Cryo-EM structures of the human PA200 and PA200-20S complex reveal regulation of proteasome gate opening and two PA200 apertures. *PLoS Biol* 2020;**18**:e3000654.
16. Berman HM, Battistuz T, Bhat TN, Bluhm WF, Bourne PE, Burkhardt K, et al. The protein data bank. *Nucleic Acids Res* 2000;**58**: 899−907.
17. Knox C, Wilson M, Klinger CM, Franklin M, Oler E, Wilson A, et al. DrugBank 6.0: the drugbank knowledgebase for 2024. *Nucleic Acids Res* 2024;**52**:D1265-75.
18. Fuhrmann J, Rurainski A, Lenhof HP, Neumann D. A new Lamarckian genetic algorithm for flexible ligand−receptor docking. *J Comput Chem* 2010;**31**:1911−8.
19. Khezri A, Karimi A, Yazdian F, Jokar M, Mofradnia SR, Rashedi H, et al. Molecular dynamic of curcumin/chitosan interaction using a computational molecular approach: emphasis on biofilm reduction. *Int J Biol Macromol* 2018;**114**:972−8.
20. Buque A, Bloy N, Perez-Lanzon M, Iribarren K, Humeau J, Pol JG, et al. Immunoprophylactic and immunotherapeutic control of hormone receptor-positive breast cancer. *Nat Commun* 2020;**11**:3819.
21. Wang JY, Li SQ, Wang J, Wu FX, Chen YH, Zhang H, et al. Spermidine alleviates cardiac aging by improving mitochondrial biogenesis and function. *Aging (Albany NY)* 2020;**12**:650−71.
22. Coni S, Serrao SM, Yurtsever ZN, Di Magno L, Bordone R, Bertani C, et al. Blockade of EIF5A hypusination limits colorectal cancer growth by inhibiting MYC elongation. *Cell Death Dis* 2020;**11**:1045.
23. Morgan DM. Determination of polyamines as their benzoylated derivatives by HPLC. *Methods Mol Biol* 1998;**79**:111−8.
24. Tang DL, Chen X, Kang R, Kroemer G. Ferroptosis: molecular mechanisms and health implications. *Cell Res* 2021;**31**:107−25.
25. Kumar V, Mishra RK, Ghose D, Kalita A, Dhiman P, Prakash A, et al. Free spermidine evokes superoxide radicals that manifest toxicity. *Elife* 2022;**11**:e77704.
26. Tonelli C, Chio IIC, Tuveson DA. Transcriptional regulation by Nrf2. *Antioxid Redox Signal* 2018;**29**:1727−45.
27. Dowdle WE, Nyfeler B, Nagel J, Elling RA, Liu S, Triantafellow E, et al. Selective VPS34 inhibitor blocks autophagy and uncovers a role for NCOA4 in ferritin degradation and iron homeostasis *in vivo*. *Nat Cell Biol* 2014;**16**:1069−79.
28. Mancias JD, Wang X, Gygi SP, Harper JW, Kimmelman AC. Quantitative proteomics identifies NCOA4 as the cargo receptor mediating ferritinophagy. *Nature* 2014;**509**:105−9.
29. Chen X, Yu CH, Kang R, Tang DL. Iron metabolism in ferroptosis. *Front Cel Dev Biol* 2020;**8**:590226.
30. Park MH, Wolff EC. Hypusine, a polyamine-derived amino acid critical for eukaryotic translation. *J Biol Chem* 2018;**293**: 18710−8.
31. Stewart D, Killeen E, Naquin R, Alam S, Alam J. Degradation of transcription factor Nrf2 *via* the ubiquitin−proteasome pathway and stabilization by cadmium. *J Biol Chem* 2003;**278**:2396−402.
32. Nguyen T, Sherratt PJ, Huang HC, Yang CS, Pickett CB. Increased protein stability as a mechanism that enhances Nrf2-mediated transcriptional activation of the antioxidant response element. *J Biol Chem* 2003;**278**:4536−41.
33. Zeng J, Ye Z, Shi S, Liang Y, Meng Q, Zhang Q, et al. Targeted inhibition of $eIF5A^{hpu}$ suppresses tumor growth and polarization of M2-like tumor-associated macrophages in oral cancer. *Cell Death Dis* 2023;**14**:579.
34. Kim HI, Schultz CR, Chandramouli GVR, Geerts D, Risinger JI, Bachmann AS. Pharmacological targeting of polyamine and hypusine biosynthesis reduces tumour activity of endometrial cancer. *J Drug Target* 2022;**30**:623−33.
35. Fang L, Gao L, Xie L, Xiao GZ. Eukaryotic translation initiation factor 5A-2 involves in doxorubicin-induced epithelial−mesenchymal transition in oral squamous cell carcinoma cells. *J Cancer* 2018;**9**: 3479−88.
36. Ulasov AV, Rosenkranz AA, Georgiev GP, Sobolev AS. Nrf2/Keap1/ARE signaling: towards specific regulation. *Life Sci* 2022;**291**: 120111.
37. Thomas TA, Smith DM. Proteasome activator 28γ (PA28γ) allosterically activates trypsin-like proteolysis by binding to the α-ring of the 20S proteasome. *J Biol Chem* 2022;**298**:102140.
38. Yazgili AS, Ebstein F, Meiners S. The proteasome activator PA200/PSME4: an emerging new player in health and disease. *Biomolecules* 2022;**12**:1150.
39. Montcusi B, Madrid-Gambin F, Marin S, Mayol X, Pascual M, Cascante M, et al. Circulating metabolic markers identify patients at risk for tumor recurrence: a prospective cohort study in colorectal cancer surgery. *Ann Surg* 2024;**280**:842−9.
40. Huang CY, Fang YJ, Abulimiti A, Yang X, Li L, Liu KY, et al. Dietary polyamines intake and risk of colorectal cancer: a case-control study. *Nutrients* 2020;**12**:3575.
41. Yue F, Li WJ, Zou J, Jiang XH, Xu GB, Huang H, et al. Spermidine prolongs lifespan and prevents liver fibrosis and hepatocellular carcinoma by activating MAP1S-mediated autophagy. *Cancer Res* 2017; **77**:2938−51.
42. Bi GS, Liang JQ, Bian YY, Shan GY, Huang YW, Lu T, et al. Polyamine-mediated ferroptosis amplification acts as a targetable vulnerability in cancer. *Nat Commun* 2024;**15**:2461.
43. Miao HM, Ou JJ, Peng Y, Zhang X, Chen YJ, Hao LJ, et al. Macrophage ABHD5 promotes colorectal cancer growth by suppressing spermidine production by SRM. *Nat Commun* 2016;**7**:11716.
44. Kiechl S, Pechlaner R, Willeit P, Notdurfter M, Paulweber B, Willeit K, et al. Higher spermidine intake is linked to lower mortality: a prospective population-based study. *Am J Clin Nutr* 2018;**108**: 371−80.

45. Zhou XM, Zou LB, Liao HY, Luo JQ, Yang TW, Wu J, et al. Abrogation of HnRNP L enhances anti-PD-1 therapy efficacy *via* diminishing PD-L1 and promoting $CD8^+$ T cell-mediated ferroptosis in castration-resistant prostate cancer. *Acta Pharm Sin B* 2022;**12**: 692−707.
46. Luo YL, Linghu MY, Luo XY, Li DD, Wang JL, Peng SJ, et al. Remodeling tumor immunosuppressive microenvironment through dual activation of immunogenic panoptosis and ferroptosis by H_2S-amplified nanoformulation to enhance cancer immunotherapy. *Acta Pharm Sin B* 2025;**15**:1242−54.
47. Lei G, Zhuang L, Gan BY. Targeting ferroptosis as a vulnerability in cancer. *Nat Rev Cancer* 2022;**22**:381−96.
48. Gamble LD, Purgato S, Murray J, Xiao L, Yu DMT, Hanssen KM, et al. Inhibition of polyamine synthesis and uptake reduces tumor progression and prolongs survival in mouse models of neuroblastoma. *Sci Transl Med* 2019;**11**:eaau1099.
49. Khan A, Gamble LD, Upton DH, Ung C, Yu DMT, Ehteda A, et al. Dual targeting of polyamine synthesis and uptake in diffuse intrinsic pontine gliomas. *Nat Commun* 2021;**12**:971.
50. Ding YH, Feng YK, Huang ZL, Zhang Y, Li X, Liu R, et al. SOX15 transcriptionally increases the function of AOC1 to modulate ferroptosis and progression in prostate cancer. *Cell Death Dis* 2022;**13**:673.
51. Niu CY, Jiang DM, Guo YN, Wang ZL, Sun Q, Wang X, et al. Spermidine suppresses oxidative stress and ferroptosis by Nrf2/HO-1/GPX4 and Akt/FHC/ACSL4 pathway to alleviate ovarian damage. *Life Sci* 2023;**332**:122109.
52. Cheng Q, Ni L, Liu A, Huang XX, Xiang P, Zhang Q, et al. Spermidine protects cartilage from IL-1β-mediated ferroptosis. *Mol Cell Biochem* 2024;**479**:2785−94.
53. Sun J, Xu JY, Liu Y, Lin YT, Wang FG, Han Y, et al. Exogenous spermidine alleviates diabetic cardiomyopathy *via* suppressing reactive oxygen species, endoplasmic reticulum stress, and Pannexin-1-mediated ferroptosis. *Biomol Biomed* 2023;**23**:825−37.
54. Youssef MAM, Mohamed TM, Bakry AA, El Keiy MM. Synergistic effect of spermidine and ciprofloxacin against Alzheimer's disease in male rat *via* ferroptosis modulation. *Int J Biol Macromol* 2024;**263**: 130387.
55. Lee H, Zandkarimi F, Zhang Y, Meena JK, Kim J, Zhuang L, et al. Energy-stress-mediated AMPK activation inhibits ferroptosis. *Nat Cell Biol* 2020;**22**:225−34.
56. Lubas M, Harder LM, Kumsta C, Tiessen I, Hansen M, Andersen JS, et al. eIF5A is required for autophagy by mediating ATG3 translation. *EMBO Rep* 2018;**19**:e46072.
57. Zhang HL, Alsaleh G, Feltham J, Sun YZ, Napolitano G, Riffelmacher T, et al. Polyamines control eIF5A hypusination, TFEB translation, and autophagy to reverse B cell senescence. *Mol Cell* 2019;**76**:110−25.e9.
58. Liu PF, de la Vega MR, Dodson M, Yue F, Shi BY, Fang D, et al. Spermidine confers liver protection by enhancing NRF2 signaling through a MAP1S-mediated noncanonical mechanism. *Hepatology* 2019;**70**:372−88.
59. Eisenberg T, Abdellatif M, Schroeder S, Primessnig U, Stekovic S, Pendl T, et al. Cardioprotection and lifespan extension by the natural polyamine spermidine. *Nat Med* 2016;**22**:1428−38.
60. Zhang Y, Bai J, Cui ZK, Li Y, Gao Q, Miao Y, et al. Polyamine metabolite spermidine rejuvenates oocyte quality by enhancing mitophagy during female reproductive aging. *Nat Aging* 2023;**3**: 1372−86.
61. Schwarz C, Stekovic S, Wirth M, Benson G, Royer P, Sigrist SJ, et al. Safety and tolerability of spermidine supplementation in mice and older adults with subjective cognitive decline. *Aging (Albany NY)* 2018;**10**:19−33.
62. Wirth M, Benson G, Schwarz C, Kobe T, Grittner U, Schmitz D, et al. The effect of spermidine on memory performance in older adults at risk for dementia: a randomized controlled trial. *Cortex* 2018;**109**: 181−8.
63. Schwarz C, Benson GS, Horn N, Wurdack K, Grittner U, Schilling R, et al. Effects of spermidine supplementation on cognition and biomarkers in older adults with subjective cognitive decline: a randomized clinical trial. *JAMA Netw Open* 2022;**5**:e2213875.